HHS Public Access

Author manuscript

Cell Rep. Author manuscript; available in PMC 2024 May 15.

Published in final edited form as:

Cell Rep. 2024 April 23; 43(4): 114007. doi:10.1016/j.celrep.2024.114007.

Insulin receptor signaling engages bladder urothelial defenses that limit urinary tract infection

Laura Schwartz[1,2,8], **Kristin Salamon**[1,8], **Aaron Simoni**[1], **Tad Eichler**[1], **Ashley R. Jackson**[1,2], **Matthew Murtha**[1], **Brian Becknell**[1,2], **Andrew Kauffman**[1,3], **Sarah Linn-Peirano**[1,4], **Natalie Holdsworth**[1,5], **Vidhi Tyagi**[1], **Hancong Tang**[1], **Steve Rust**[1], **Hanna Cortado**[1], **Irina Zabbarova**[6], **Anthony Kanai**[6,7], **John David Spencer**[1,2,9,*]

[1]The Kidney and Urinary Tract Center, The Abigail Wexner Research Institute at Nationwide Children's, Columbus, OH 43205, USA

[2]Division of Nephrology and Hypertension, Nationwide Children's, Columbus, OH 43205, USA

[3]Tulane University, New Orleans, LA 70118, USA

[4]Department of Veterinary Biosciences, The Ohio State University College of Veterinary Medicine, Columbus, OH 43210, USA

[5]Ohio University Heritage College of Osteopathic Medicine, Athens, OH 45701, USA

[6]Department of Medicine, Renal-Electrolyte Division, University of Pittsburgh School of Medicine, Pittsburgh, PA 15213, USA

[7]Department of Pharmacology and Chemical Biology, University of Pittsburgh School of Medicine, Pittsburgh, PA 15213, USA

[8]These authors contributed equally

[9]Lead contact

SUMMARY

Urinary tract infections (UTIs) commonly afflict people with diabetes. To better understand the mechanisms that predispose diabetics to UTIs, we employ diabetic mouse models and altered insulin signaling to show that insulin receptor (IR) shapes UTI defenses. Our findings are validated in human biosamples. We report that diabetic mice have suppressed IR expression and are more susceptible to UTIs caused by uropathogenic *Escherichia coli* (UPEC). Systemic

*Correspondence: john.spencer@nationwidechildrens.org.

AUTHOR CONTRIBUTIONS

L.S. and J.D.S. supervised the project and contributed to the design and interpretation of all experiments. K.S. and M.M. managed the mouse colony. K.S. and M.M. performed the *in vivo* mouse experiments. K.S. and A.S. performed genotyping and real-time PCR. S.L.-P., A.R.J., H.C., and B.B. completed the histopathology scoring, immunostaining, *in situ* hybridization, flow cytometry, or microscopy. L.S., V.T., A.K., T.E., and J.D.S. performed the *in vitro* experiments or western blots. N.H. and V.T. performed the ELISAs. H.T. and S.R. performed the statistical analysis. A.K. and I.Z. completed the Ussing chamber experiments. L.S., K.S., and J.D.S. wrote the manuscript with input from all authors.

DECLARATION OF INTERESTS

The authors declare no competing interests.

SUPPLEMENTAL INFORMATION

Supplemental information can be found online at https://doi.org/10.1016/j.celrep.2024.114007.

IR inhibition increases UPEC susceptibility, while IR activation reduces UTIs. Localized IR deletion in bladder urothelium promotes UTI by increasing barrier permeability and suppressing antimicrobial peptides. Mechanistically, IR deletion reduces nuclear factor κB (NF-κB)-dependent programming that co-regulates urothelial tight junction integrity and antimicrobial peptides. Exfoliated urothelial cells or urine samples from diabetic youths show suppressed expression of IR, barrier genes, and antimicrobial peptides. These observations demonstrate that urothelial insulin signaling has a role in UTI prevention and link IR to urothelial barrier maintenance and antimicrobial peptide expression.

In brief

Schwartz et al. define the significance of insulin receptor signaling in the bladder urothelium during urinary tract infection. Insulin receptor engages downstream targets, including NF-κB, to maintain the urothelial barrier and expression of host defense peptides that prevent infection.

Graphical Abstract

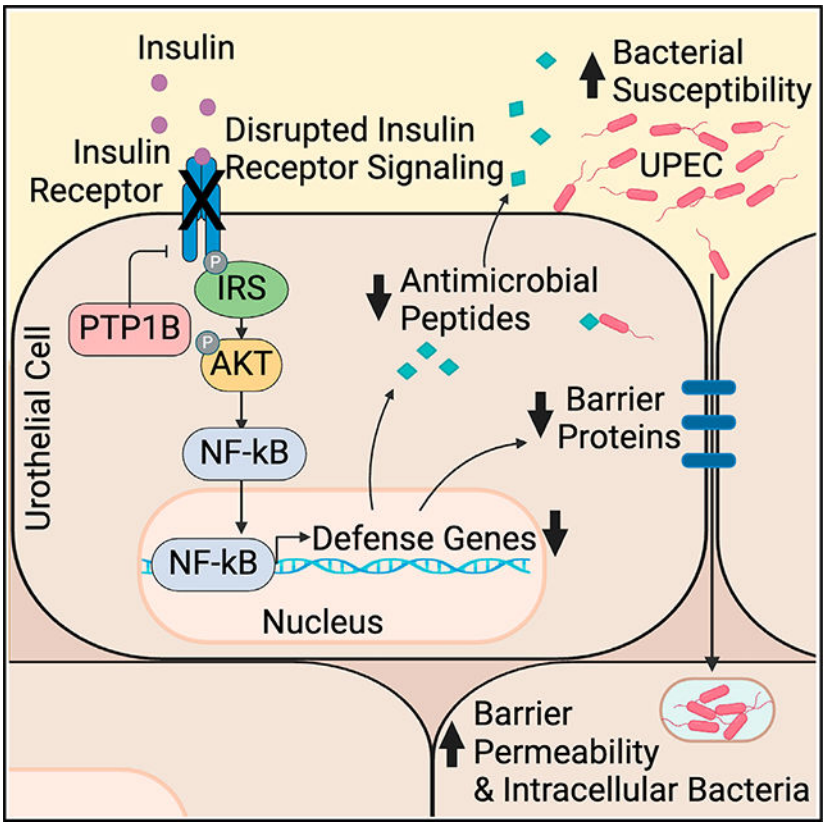

INTRODUCTION

Type 2 diabetes is associated with increased infection risk, and urinary tract infections (UTIs) are 10 times more common in people with diabetes.[1,2] In diabetic populations, the risk of bacteremia with UTI is 4 times greater, and UTI mortality rates are 5 times greater.[2–5] Because of the growing global incidence of diabetes and this heightened susceptibility

to UTI, diabetes-associated UTI management places a substantial burden on the healthcare system.[1] Understanding why people with diabetes are predisposed to UTI may lead to approaches that improve clinical outcomes and reduce healthcare costs.

Uropathogenic *Escherichia coli* (UPEC) is the most common UTI-inciting pathogen. UPEC originates from the fecal microbiota, spreads across the perineum, and enters the bladder through the urethra. Within the bladder, UPEC binds to and invades superficial urothelial cells. The urothelium is a stratified epithelium composed of three layers. The superficial layer consists of terminally differentiated umbrella cells that establish a barrier to waste, water, urinary solutes, and pathogens. It includes an apical plaque composed of uroplakins and a paracellular junctional complex comprised of tight junctions, adherens junctions, and desmosomes. The intermediate layer contains partially differentiated cells that can differentiate into superficial cells. The basal layer is the least differentiated and contains keratin 5or 14-expressing cells that are a source of urothelial renewal.[6–8] To establish infection, UPEC overcomes diverse urothelial defenses, including the urothelial barrier, activation of pattern recognition receptors, cytokine and chemokine production that attracts leukocytes, and the secretion of antimicrobial peptides that kill invading pathogens.[9,10] Our understanding of how diabetes impacts these defenses is a knowledge gap.

Impaired glucose control is traditionally regarded as the driver of diabetes-associated UTI. Elevated blood or urinary glucose concentrations can attenuate urothelial chemokine and antimicrobial peptide production, reduce phagocyte infiltration, facilitate UPEC binding to urothelial cells, and compromise barrier integrity.[3,11–15] However, evidence suggests that insulin resistance may heighten UTI susceptibility before the onset of hyperglycemia or glucosuria.[16–18] These findings suggest that the hyperglycemic environment may not fully explain diabetes-associated UTI, emphasizing a potential role of insulin bioavailability in shaping UTI susceptibility.

Insulin is vital for glucose metabolism, gene transcription, protein synthesis, cell proliferation, and survival. Insulin's actions are mediated by its receptor. When complexed to insulin, insulin receptor (IR) undergoes a conformational change that initiates its kinase activity to engage downstream nodes that control metabolism and cellular functions. Inefficient IR signaling, a decrease in the number of functional receptors, and/or aberrant post-IR signaling, promote insulin resistance, the primary abnormality leading to type 2 diabetes.[19–21] While IR is expressed in most organ systems, it has been thoroughly characterized in adipose tissue, liver, and skeletal muscle. IR deletion in these insulin-responsive organs establishes insulin resistance.[22–25]

The effects of impaired IR signaling extend beyond insulin resistance and defective glucose regulation. Tissue-specific IR deletion affects lipid metabolism, obesity, blood pressure, behavior, fertility, and immunity.[26,27] IR deletion in intestinal Paneth cells and kidney collecting duct cells suppresses antimicrobial peptide expression, macrophages lacking IR exhibit reduced responsiveness to pathogens and have suppressed cytokine production, and IR-deficient T cells display reduced immunity against influenza.[16,28–31] The effects of insulin and IR signaling in the bladder urothelium have not been investigated. Additionally, it is unknown whether diabetes impacts urothelial IR expression or whether deregulated

urothelial IR signaling contributes to UTI pathogenesis. To address these knowledge gaps, we employ diabetic mice, murine models of systemic IR inhibition and activation, and urothelium-specific IR knockout mice to define the role of insulin and IR signaling on UTI defenses. Our preclinical findings are validated in human urothelial cultures and biological samples collected from healthy children and youths with type 2 diabetes. Using these complementary and translational models, we uncover an important role of IR in maintaining the urothelial barrier and regulating innate defenses that prevent UTI.

RESULTS

Type 2 diabetes mellitus increases susceptibility to UPEC

To ensure diabetes heightens UTI risk, we transurethrally infected female diabetic *ob*/*ob* mice and non-diabetic *ob*/+ mice with UPEC. Leptin-deficient *ob*/*ob* mice are obese and hyperglycemic and have elevated urinary glucose and serum insulin concentrations (Figures 1A–1D). Compared with controls, o*b*/*ob* mice have suppressed bladder IR expression (Figure 1E). After UTI, *ob*/*ob* mice have significantly greater urinary and bladder UPEC titers compared with controls (Figure 1F). These results verify that type 2 diabetic mice have increased UPEC susceptibility and suggest that impaired IR signaling may promote UTI.

Systemic IR inhibition promotes UTI

To assess the impact of IR on UTI defense, we treated mice with OSI-906, an insulin growth factor 1 receptor (IGF1R) and IR antagonist (Figure S1A). Pharmacokinetics data demonstrate that lower OSI-906 doses (30 mg/kg) inhibit IGF1R phosphorylation, while higher OSI-906 doses (60 mg/kg) inhibit both IGF1R and IR phosphorylation *in vivo*.[32] Female mice were treated twice with vehicle or OSI-906 (30 mg/kg or 60 mg/kg) and transurethrally infected with UPEC (Figure 2A). Western blotting confirms that OSI-906 administration inhibits bladder IGF1R/IRβ phosphorylation and activation of its downstream target AKT (Figure 2B). Blood glucose concentrations were similar in mice treated with vehicle or 30 mg/kg OSI-906, while mice treated with 60 mg/kg OSI-906 developed hyperglycemia and glucosuria, confirming that higher-dose OSI-906 inhibits IR (Figure 2C). Following UTI, mice treated with vehicle and 30 mg/kg OSI-906 had comparable urinary and bladder UPEC titers. In contrast, mice treated with 60 mg/kg OSI-906 had a significantly greater urine and bladder UPEC burden (Figure 2D), indicating that IR inhibition may be a UTI risk factor, while IGF1R inhibition may not have as significant a role. When we compared the urinary and bladder UPEC burden with blood glucose concentrations in mice receiving 60 mg/kg OSI-906, no correlation was observed between bacterial colony-forming units and glucose concentrations (Figure S2).

To circumvent the confounding effects of hyperglycemia or glucosuria, we performed a second experiment and treated mice with one dose of OSI-906 (60 mg/kg) or vehicle before infecting them with UPEC (Figure 2E). Western blotting confirms that OSI-906 treatment inhibits bladder IR signaling (Figure 2F). Vehicle- and OSI-906 treated mice had similar blood and urinary glucose concentrations (Figure 2G). Despite having comparable glucose control, OSI-906-treated mice had 2-fold greater urinary and bladder UPEC burdens 24 h

after infection compared with vehicle-treated mice (Figure 2H). These results suggest that impaired IR signaling, independent of abnormal glucose control, increases UTI.

Inhibiting IR in human urothelial cells promotes infection

To assess the translational potential of these findings, we treated primary human urothelial cells with OSI-906. Western blotting confirmed inhibition of IR signaling following OSI-906 treatment (Figure 2I). Next, we challenged vehicle- and OSI-906-treated cells with UPEC. With OSI-906 treatment, the percentage of bacteria binding to the cellular surface or invading the cells increased (Figures 2J and S3). Similar results were observed using human 5637 and T24 urothelial cells (Figure S4). To validate that this finding is specific to impaired IR signaling, primary human urothelial cells were transfected with an IR or non-targeting control small interfering RNA (siRNA) pool. When *INSR* was silenced, the percentage of UPEC binding or invading the cells increased (Figures 2K, 2L, and S3). These results provide supporting evidence that IR is necessary to prevent UPEC infection.

Systemic IR activation reduces UTI susceptibility

Protein tyrosine phosphatase 1B (PTP1B) is an endoplasmic reticulum-targeted phosphatase that dephosphorylates and inactivates IR (Figure S1A).[33,34] PTP1B-deficient mice (*PTP1B*$^{-/-}$) have heightened insulin sensitivity due to enhanced IR activity.[35,36] Thus, we employed *PTP1B*$^{-/-}$ mice to test whether IR activation reduces UTI. In *PTP1B*$^{-/-}$ mice, real-time PCR confirmed that PTP1B transcript deletion and immunostaining did not detect PTP1B production in bladder urothelium (Figures 3A and 3B). Compared with controls (*PTP1B*$^{+/+}$), female *PTP1B*$^{-/-}$ mice had reduced body weight, similar insulin concentrations, and an augmented ability to clear glucose from their peripheral circulation during intraperitoneal glucose tolerance tests (Figures 3C–3E). Twenty-four hours after UTI, female *PTP1B*$^{-/-}$ mice had significantly lower bladder and urinary UPEC burdens compared with controls (Figure 3F). Similar results were observed in male *PTP1B*$^{-/-}$ mice (Figure S5).

Activating urothelial IR signaling prevents infection

To determine whether urothelial IR activation reduces UPEC susceptibility, we isolated and cultured bladder urothelium from *PTP1B*$^{-/-}$ mice and controls *ex vivo*. Urothelium from PT^{-}P1B$^{-/-}$ mice showed enhanced insulin sensitivity (Figure 3G). Following UPEC infection, the percentage of UPEC-binding or invading *PTP1B*$^{-/-}$ urothelial cells was significantly lower than *PTP1B*$^{+/+}$ urothelial cells (Figures 3H and S6). To validate this finding, human urothelial cells were transfected with a PTP1B or non-targeting control siRNA pool. Silencing *PTP1B* augmented IR signaling and reduced UPEC infection, indicating that urothelial IR activation decreases UPEC susceptibility (Figures 3I–3K and S6).

Generation and characterization of urothelium-specific IR knockout mice

To mechanistically define how IR affects bladder antibacterial defenses, we deleted IR in the superficial and intermediate or basal urothelial cell layers. Single-cell RNA sequencing data and immunohistochemical staining demonstrate that IR is expressed throughout the urothelium (Figures S1B–S1D).[17,37] To delete IR in superficial and intermediate bladder

urothelial cells, mice homozygous for the floxed *Insr* gene (*Insr*$^{fl/fl}$) were bred with uroplakin 2 Cre/ERT2 mice (Upk2-iCre; Figure 4A).[25,38] To delete IR in basal urothelial cells, *Insr*$^{fl/fl}$ mice were crossed with keratin 5 Cre/ERT2 mice (Krt5-iCre; Figure S7A).[39] We incorporated a tdTomato (tdT) fluorescent reporter strain to visualize Cre-mediated recombination. Throughout this manuscript, mice with IR deletion are referenced as IRKO, and homozygous floxed littermates lacking the Cre transgene are referred to as IRflox.

PCR confirmed Cre-mediated recombination in bladder urothelium isolated from Upk2-iCre or Krt5-iCre IRKO mice, and immunofluorescent staining localized tdT expression to the Cre-targeted urothelial cell layer(s) (Figures 4A, 4B, S7A, and S7B). We were unable to visualize IR deletion with immunostaining due to the lack of commercially available antibodies specific to the deleted IRb epitope. Thus, we employed *in situ* hybridization using probes specific to exons 3–5 of the *Insr* gene that are deleted with Cre recombination. In control mice, *Insr* expression was visualized in all urothelial cell layers. In Upk2-iCre IRKO mice, *Insr* expression was diminished in superficial and intermediate cells, but it was detected in basal cells (Figure 4B). In support of this finding, real-time PCR showed reduced *Insr* transcript expression in urothelium isolated from Upk2-iCre and Krt5-iCre IRKO mice (Figures 4C and S7C). Upk2-iCre and Krt5-iCre IRKO mice had normal phenotypes, bladder histopathology, serum insulin concentrations, and no evidence of hyperglycemia or glucosuria (Figures 4D–4F and S7D–S7F). To test whether IR deletion impacts cell viability, we performed terminal deoxynucleotidyl transferase dUTP nick end labeling (TUNEL) staining and did not observe differences in apoptosis between IRKO and IRflox bladders (Figure S8).

IR deletion in suprabasal urothelial cells increases UPEC susceptibility

To interrogate whether IR deletion affects UTI susceptibility, we infected female IRflox and IRKO mice with UPEC. Six hours following infection, significantly more intracellular bacterial communities were enumerated in the bladders from Upk2-iCre IRKO mice (Figure 4G). Twenty-four hours after infection, Upk2-iCre IRKO mice had significantly greater UPEC titers in the urine and bladder compared with controls (Figure 4H). In contrast, Krt5-iCre IRKO and IRflox mice had comparable bacterial burdens (Figure S7G). To determine whether Upk2-iCre IRKO mice show sustained susceptibility to UPEC, we enumerated urinary and bladder UPEC titers 48 and 72 h after infection. Compared with controls, Upk2-iCre IRKO mice continued to demonstrate greater UPEC urinary and bladder titers at these time points (Figure 4H). Gross and histopathological analyses of a subset of bladders from Upk2-iCre IRKO mice showed that the infected bladders were more edematous and inflamed compared with controls, indicative of more severe infection (Figures S9A–S9D). These differences in bladder pathology were not observed in Krt5-iCre IRKO mice (Figure S9E). These results suggest that IR signaling in superficial and intermediate urothelial cells is critical to shield the urothelium from UPEC. They also indicate that IR signaling in the basal urothelium may not play a role in acute UTI defense.

IR deletion in suprabasal urothelial cells compromises the urothelial barrier

Because a major function of the urothelium is to form an impermeable barrier to UPEC, we postulated that IR deletion in suprabasal cells compromises barrier integrity. Thus, we

profiled the expression of uroplakin and barrier genes and proteins maintaining the apical membrane and junctional complex in control and IRKO mice. We identified comparable uroplakin transcript and protein expression in IRflox and IRKO mouse urothelium, suggesting that IR deletion does not affect uroplakin expression (Figures 4B, S7B, and S10). Among the 13 junctional complex genes profiled in in IRKO and IRflox urothelium, we observed significantly suppressed *Cldn4*, *Cldn8*, *Tjp1*, *Cdh1*, *Dsg3*, and *Dsc2* expression in Upk2-iCre IRKO mice (Figure 5A; Table S1). In support of this finding, western blotting identified decreased E-cadherin, claudin 4, and claudin 8 expression in Upk2-iCre IRKO urothelium (Figure 5B). We were unable to routinely detect ZO-1, desmoglein 3, or desmocollin 2 via western blot. In Krt5-iCre IRKO mice, we observed suppressed expression of *Dsc2* and *Dsc3*, while the expression of the other genes did not differ (Figure S11A). These findings indicate that IR deletion in apical and intermediate cells suppresses structural genes and proteins that maintain the urothelial barrier.

To quantify the effect of IR deletion on urothelial architecture and function, we visualized the apical membrane and junctional complex and observed widened paracellular spaces and an absence of defined junctional complexes along the lateral cellular surfaces in Upk2-iCre IRKO mice (Figure 5C). Next, we measured urothelial transepithelial resistance (TER) and permeability to radiolabeled water and urea in bladders mounted within Ussing chambers. Bladders from Upk2-iCre IRKO mice showed a significant decrease in TER as well as an increase in permeability to water and urea compared with controls (Figure 5D). Krt5-iCre IRKO mice showed no change in TER or water/urea permeability (Figure S11B). These results support our hypothesis that IR deletion in superficial and intermediate cells perturbs urothelial barrier integrity while also insinuating that IR deletion in basal cells does not compromise barrier function.

Disrupting the urothelial barrier in human bladder cells promotes UPEC infection

To validate this finding in human urothelium, we silenced *INSR* expression using siRNA. With *INSR* silencing, we observed suppressed expression of urothelial barrier genes encoding ZO-1, E-cadherin, and claudin 4 (Figure 5E). Next, we cultured human urothelial cells on permeable membranes and assessed the permeability of fluorescein isothiocyanate (FITC)-conjugated dextran when applied to the apical surface of confluent cells. Cellular permeability to low-molecular-weight dextran increased with *INSR* silencing, as evidenced by increased FITC-dextran fluorescence in the basal chamber (Figure 5F). Similar results were observed in OSI-906 treated 5637 and T24 urothelial cells (Figure S12), confirming that deregulated IR signaling disrupts the urothelial barrier.

Next, we assessed the contributions of these individual genes to barrier integrity by culturing primary human urothelial cells on Transwells and transfecting them with a *CDH1*, *CLDN4*, *TJP1*, or a non-targeting control siRNA pool. Real-time PCR confirmed target gene knockdown (Figure 5G). When these genes were silenced, permeability to FITC-dextran increased (Figure 5H). Because diminished barrier function may facilitate UTI, we analyzed the capacity of UPEC to translocate across and invade human urothelial cells with intact and silenced junctional complexes. When *CDH1*, *CLDN4*, and *TJP1* were silenced, apical-to-basal UPEC translocation increased as greater UPEC titers were recovered in the

basal chamber medium (Figure 5I). Similarly, UPEC invasion significantly increased when *CLDN4* and *TJP1* were silenced (Figure 5J). Collectively, these experiments underscore that deregulating IR and disrupting the urothelial barrier potentiates UTI.

IR deletion suppresses urothelial immune defenses

Evidence also suggests that insulin regulates immune responses and antimicrobial peptide expression.[16–18] Therefore, we assessed the expression of immune genes and antimicrobial peptides in urothelium isolated from non-infected IRflox and Upk2-iCre IRKO bladders. Of the 87 profiled genes, 50 genes exhibited 1.5-fold or greater suppressed expression in IRKO urothelium (Table S2). The differentially expressed genes were categorized into four unique groups: antimicrobial peptides (group 1), antibacterial signaling responses (group 2), non-obese diabetic (NOD)-like receptor signaling (group 3), and Toll-like receptor signaling (group 4) (Figure 6A). Suppressed expression of these genes was not detected in non-infected Krt5-iCre IRKO urothelium (Figure S11C).

To test the impact of IR deletion on these immune defenses during UPEC infection, we profiled antimicrobial peptide expression (group 1) in urothelium isolated from infected IRflox and Upk2-iCre mouse bladders. With UPEC infection, we observed significantly suppressed *Lcn2*, *Hamp*, *Rnase4*, and *Slpi* transcript expression in IRKO urothelium, while the expression of *Defb1*, *Camp*, and *Dmbt1* was similar in infected IRflox and IRKO urothelium, indicating that a subgroup of antimicrobial peptides is regulated by IR signaling (Figures 6B and S13).

Since several nuclear factor κB (NF-κB) target genes were suppressed in IRKO urothelium (group 2), we performed immunostaining for NF-κB p65 on bladders collected from IRflox and Upk2-iCre mice. Non-infected IRflox and IRKO bladders showed no discernable NF-κB p65 expression (Figure S14). In UPEC-challenged IRflox mice, we observed cytoplasmic NF-κB p65 expression throughout the urothelium as well as nuclear NF-κB p65 staining that was most pronounced in apical urothelial cells (Figures 6D and S14). NF-κB expression was most prominent 24 h after infection and not routinely detected 48 h after UTI (Figure S14). In Upk2-iCre IRKO infected mice, we observed cytoplasmic NF-κB p65 expression in basal urothelial cells, but we did not routinely detect cytoplasmic or nuclear p65 expression in the suprabasal cells, suggesting that cells lacking IR cannot activate NF-κB (Figure 6C). Furthermore, we noted suppressed expression of a subset of NF-κB target genes following infection (Figure S15). Because NF-κB target genes can influence immune cell recruitment to sites of infection, we profiled phagocyte cell populations in UPEC-infected bladders using flow cytometry. Twenty-four hours after infection, we observed comparable neutrophil, monocyte, and macrophage profiles in control and Upk2-iCre IRKO bladders (Figure S16).

To define how IR regulates immune responses in human urothelium, human urothelial cells were transfected with a siRNA pool targeting *INSR*. With INSR silencing, we detected suppressed antimicrobial peptide expression (Figure 6D). To assess how IR affects NF-κB, we silenced *INSR* in human urothelial cells and challenged them with UPEC. Western blotting shows that control cells exhibited heightened NF-κB activity upon UPEC exposure, while cells with reduced *INSR* expression displayed attenuated NF-κB activation (Figure

6E). To further investigate whether IR controls NF-κB activity through its downstream mediator AKT, which is suppressed with deregulated IR activity (Figures 2 and 5B), we silenced *AKT1* using siRNA. Silencing *AKT1* lead to decreased NF-κB before and after UPEC infection. Western blotting demonstrates that NF-κB is suppressed because *INSR* and *AKT1* silencing prevents degradation of the NF-κβ inhibitor IκBα (Figure 6E). To corroborate these findings, human urothelial cells were co-transfected with siRNA and a reporter plasmid encoding firefly luciferase downstream of an NF-κB response element, allowing for quantification of NF-κB activity. Before and after UPEC challenge, cells with reduced *INSR* or *AKT1* expression exhibited diminished NF-κB luciferase activity compared with controls (Figures 6E and S17). Similar trends were observed in OSI-906-treated cells (Figure S18). Together, these findings indicate that deregulated IR signaling and reduced AKT expression compromise NF-κB activity.

NF-κB maintains urothelial barrier integrity and regulates antimicrobial peptide expression

To test whether NF-κB controls the expression of antimicrobial peptide or barrier genes, human urothelial cells were transfected with a *NFKB1* or non-targeting control siRNA pool and challenged with UPEC. Following *NFKB1* silencing, we observed suppressed *LCN2*, *RNASE4*, *RNASE7*, *CDH1*, and *TJP1* expression before and after UPEC challenge (Figure 6E). The expression of *DEFB1*, *SLPI*, and *CLDN4* was not affected by *NFKB1* silencing. To validate the role of the NF-κB transcription factor complex in regulating the expression of these genes, we performed chromatin immunoprecipitation (ChIP) to localize NF-κB to their promoters. In non-infected cells, we observed weak NF-κB p65 binding at the *LCN2*, *RNASE4*, *RNASE7*, *CDH1*, and *TJP1* promoters. In UPEC-challenged cells, we observed increased NF-κB p65 binding. OSI-906 pretreatment reduced NF-κB p65 binding to these gene promoters with infection (Figure 6F), insinuating that IR regulates the capacity of NF-κB to jointly engage antimicrobial peptides and barrier genes.

Youths with type 2 diabetes have suppressed urothelial and urinary antibacterial defenses

Finally, we investigated whether IR expression, the urothelial barrier, and antimicrobial peptides are impaired in people with type 2 diabetes. To this end, we collected urine samples from healthy children as well as youths with type 2 diabetes (Table S3). Compared with healthy controls, exfoliated urinary cells from diabetic youths had suppressed IR mRNA expression as well as downregulated barrier gene and antimicrobial peptide expression (Figures 7A–7C). Urinary uroplakin 2 concentrations, normalized to urinary creatinine, were 1.4-fold higher in youths with diabetes, suggestive of an impaired urothelial barrier. Similarly, median urinary Lcn 2, RNase 4, and RNase 7 concentrations, normalized to urinary creatinine, were 1.2- to 2.5-fold lower in diabetic youths (Figure 7D). Similar trends were observed when uroplakin 2 and antimicrobial peptide concentrations were not normalized to urine creatinine (Table S3). These data support our preclinical findings that IR is suppressed with diabetes and may potentially drive urothelial barrier functions and antimicrobial peptide expression.

DISCUSSION

UTIs are common with diabetes, yet the mechanisms augmenting UTI risk are unclear. This study provides evidence that IR shapes UTI susceptibility. Our primary outcomes reveal that IR is downregulated in diabetic mouse bladders and exfoliated diabetic human urothelial cells, systemic and urothelial IR inhibition potentiates UTI, and IR activation reduces infection susceptibility. These findings are significant because they define a mechanism that can explain why people with diabetes are more susceptible to UTI. Additionally, they establish a foundation for targeted approaches that augment IR signaling to reduce UPEC susceptibility. Our secondary outcomes begin to delineate IR-mediated urothelial targets. We report that IR signaling in superficial and intermediate cells is necessary to maintain barrier integrity and produce antimicrobial peptides, while IR signaling in basal urothelial cells is dispensable for acute UTI defense. IR regulates these defenses, which are weakened in people with diabetes, by engaging NF-κB, establishing the IR-NF-κB-urothelial barrier/antimicrobial peptide axis as an important node regulating UTI defenses.

Historically, diabetes-associated infections are ascribed to hyperglycemia and glucosuria. In this respect, we demonstrate that *ob*/*ob* mice, with significant hyperglycemia and glucosuria, have heightened UPEC susceptibility. Similarly, published data show that diabetic *db*/*db* mice are predisposed to UTI.[15,16] While these results establish the consequence of uncontrolled diabetes on UPEC susceptibility, UTI vulnerability may develop prior to diabetes onset. In support of this concept, data show that insulin-resistant prediabetic mice are predisposed to UTI.[16] Here, our results demonstrate that pharmacologic IR inhibition and urothelial IR deletion promote insulin resistance and enhance UPEC susceptibility. Use of IR inhibitors and the IRKO model offers a unique opportunity to analyze insulin's impact on antibacterial defenses at a global and tissue-specific level without the confounding effects of abnormal glucose control or obesity.[23,25] These findings illustrate that hyperglycemia and glucosuria may not completely account for infections associated with diabetes and establish insulin resistance as a prime UTI risk factor.

Complementary to these findings, we show that global PTP1B deletion and urothelial PTP1B silencing reduce UPEC susceptibility. Like our findings, data show that mice lacking PTP1B exhibit enhanced insulin sensitivity attributable to increased IR phosphorylation.[35,36] Therefore, PTP1B is considered a fresh therapeutic option for insulin resistance, and large pharmaceutical companies are developing PTP1B inhibitors as therapies for diabetes and metabolic syndrome.[40–44] Limited evidence does implicate PTP1B in the coordination of inflammatory responses and immunity.[45–47] Given our findings, studies are needed to test how PTP1B inhibitors or urothelium-specific PTP1B deletion impacts bladder immunity. These studies may lead to unique approaches that mitigate UTI in insulin-resistant or diabetic populations.

To facilitate these studies, we illustrate that IR signaling in suprabasal cells maintains the urothelial barrier. Prior data show that diabetes compromises epithelial barriers in the brain, skin, and intestine, facilitating permeability to solutes, organic compounds, and pathogens.[48–52] Additionally, UPEC can disrupt urothelial barriers and exploit this damage to facilitate invasion.[53] Although the diabetes-associated mechanisms impairing

barrier function are not defined, evidence points to a multitude of factors, including excessive inflammation, deregulated immune responses, lipotoxicity, dysbiosis, and hyperglycemia.[52,54] In the bladder, preclinical evidence suggests that hyperglycemia compromises barrier integrity, and exfoliated human urinary cells show suppressed expression of the tight junction protein occludin.[13–15,55,56] Here, we show a direct relationship between IR impairment and urothelial permeability to solutes and pathogens. These findings suggest that heightened UTI risk may develop with deregulated IR signaling.

Our current results also demonstrate that disrupted IR signaling suppresses antimicrobial peptide expression and that diabetic youths have lower urinary antimicrobial peptide concentrations. Deficient expression of antimicrobial peptides like cathelicidin; alpha defensins; iron-regulatory proteins, including hepcidin or Lcn 2; and ribonuclease A superfamily members promotes UTI.[57–62] Cohort studies suggest that people with diabetes have suppressed serum or urinary concentrations of beta defensin 1, cathelicidin, Lcn 2, RNase 4, or RNase 7 and that the expression of some of these antimicrobial peptides may be impacted by insulin bioavailability.[16,17,63] Data demonstrate suppressed expression of the antimicrobial peptide psoriasin in diabetic rodent bladders and human samples.[15] Collectively, these findings imply the need for a prospective analysis to identify how the progression from insulin resistance to prediabetes and diabetes impacts antimicrobial peptide expression. Studies like these may identify biomarkers for people at risk for UTI. People identified as high risk may benefit from frequent clinical monitoring, tighter glucose regulation, insulin-sensitizing agents, or approaches that activate IR to augment barrier and antimicrobial peptide expression.

Last, we identify NF-κB as an important regulator of urothelial immunity. Prior data show that the mouse urothelium responds to UPEC by triggering NF-κB in superficial cells, which activates immune responses to clear UPEC.[6,64] Here, we show that IR deletion in murine suprabasal cells or inhibition in human urothelial cells suppresses AKT and canonical NF-κB activation. Like prior studies, our findings indicate that AKT regulates NF-κB, at least partially, through degradation of the NF-κB inhibitor IκB.[65,66] We also show that NF-κB silencing results in the suppression of antimicrobial peptides and urothelial barrier genes, which NF-κB regulates by binding their respective promoters. Although NF-κB binding to the DNA sequences of select cytokines has been described in response to UPEC infection, we believe these are the initial data to show the necessity of NF-κB in synergistically regulating antimicrobial peptides and barrier genes. These results are noteworthy because they identify NF-κB as another node that can be targeted to prevent or treat UTI. This must be approached with caution, as sustained NF-κB may heighten inflammation and compromise urothelial integrity.[64]

Limitations of the study

A strength of the present study is the integration of complementary mouse models, human *in vitro* assays, and clinical samples to establish a role for IR in urothelial antibacterial defenses. Despite these strengths, certain limitations warrant consideration. Our utilization of a transurethral mouse UTI model, along with a single UPEC strain, may not precisely replicate UTI pathogenesis in humans. Furthermore, the use of mice on a C57BL/6 genetic

background, traditionally resistant to recurrent infections and pyelonephritis, limit our investigations of the role of IR in preventing recurrent UTI or pyelonephritis.[67,68] Although our study demonstrates the involvement of IR in regulating the urothelial barrier, NF-κB, and antimicrobial peptides, a more comprehensive, unbiased genomics or metabolomics study could uncover additional mechanisms. Last, the generalizability of our human findings is limited by the small, cross-sectional nature of our enrollment from a single center. The extension of these outcomes to patients in different countries or adults with longer-standing diabetes and co-morbid conditions remains uncertain.

To conclude, the implications of this study are paramount for understanding the mechanisms underlying diabetes-associated infections. The present study evolves our understanding of the mechanisms underlying UTI by identifying IR as a critical regulator of urothelial defenses. Mechanistically, this study provides the evidence that IR deletion in suprabasal cells increases UTI risk by suppressing NF-κB, in turn impairing the urothelial barrier and suppressing antimicrobial peptides. Collectively, these findings elucidate a critical role of the IR and downstream NF-κB activity in urothelial defenses against UPEC.

STAR★METHODS

RESOURCE AVAILABILITY

Lead contact—Further information and requests for resources and reagents should be directed to and will be fulfilled by the lead contact, Dr. Laura Schwartz (laura.schwartz@nationwidechildrens.org).

Materials availability—This study did not generate new unique agents.

Data and code availability

- All data reported in this paper will be shared by the lead contact upon request.
- This paper does not report original code.
- Any additional information required to reanalyze the data reported in this paper is available from the lead contact upon request.

EXPERIMENTAL MODELS AND SUBJECT PARTICIPANT DETAILS

Mice—Mouse experiments were performed in accordance with Institutional Animal Care and Use Committee rules and regulations. All mice were maintained on standard rodent chow *ad libitum* with free access to water under controlled temperature and humidity with 12-h light and dark cycles. Female *ob/ob*, *ob*/+ controls, and C3H/HeOuJ mice were purchased from Jackson Laboratory (Bar Harbor, ME, USA). Male and female PTP1B null mice, floxed *Insr* mice, and mice expressing a tdTomato reporter were purchased from Jackson Laboratory. These mice are on a C56BL/6J background. Throughout the results section, experimental and control mice, mouse age, and sex are outlined. PTP1B null mice have a targeted deletion of the ATG-coding region in exon 1 of the *Ptpn1* gene.[35] Insulin receptor knock-out mice were generated by crossing mice homozygous for the floxed *Insr* gene and a tdTomato reporter with tamoxifen inducible Upk2-iCre or

Krt5-iCre mice (Jackson Laboratory). Cre(+);*Insr*$^{fl/+}$ progeny were bred with *Insr*$^{fl/fl}$ mice, generating Cre(+);*Insr*$^{fl/fl}$ *and* Cre(−);*Insr*$^{fl/fl}$ offspring. At 6 weeks of age, Cre positive and negative offspring received three doses of intraperitoneal tamoxifen dissolved in corn oil (100 mg/kg, Cayman Chemical).[70,71] Following a one-week tamoxifen wash-out period, mice were subjected to downstream studies. Genetically modified mice were genotyped according to published protocols.[25,35] Genotyping primers are listed in Table S4.

Human participants and clinical specimen collection—Human subjects research was performed in accordance with the principles of the World Medical Association's Declaration of Helsinki and the Nationwide Children's Institutional Review Board approved this study. Informed written consent was obtained from all patients. Written parental/guardian consent and patient assent were obtained for subjects less than 18 years of age. Free voided urine specimens were collected from healthy children and youth with type 2 diabetes. Patients were identified and consented in 2021 and 2022 through the Nationwide Children's diabetes, nephrology, or primary care clinics. Because the incidence of UTI is greater in females compared to males, enrollment favored females. Exclusion criteria consisted of pregnancy, institutionalized individuals, a known immunodeficiency, malignancy, use of immunosuppressant medications, chronic antibiotic use or antibiotic treatment within 1 month of enrollment, impaired kidney function, kidney or urinary tract anomalies (including hydronephrosis, solitary kidney, renal dysplasia, cystic kidney disease, urinary tract obstruction, or neurogenic bladder), or vesicoureteral reflux. Detailed information on the enrolled human subjects is outlined in Table S3. Urine specimens were collected with Assay Assure (Thermo-Fisher, Waltham, MA, USA). Following centrifugation, the urinary supernatant and cellular fractions were isolated and stored at −80°C. Urinary samples were used for ELISAs and RNA was isolated from the cellular fractions.

Human and mouse cell culture—Human 5637 (ATCC, HTB-9) and T24 (ATCC, HTB-4) cells were cultured in RPMI-1640 medium containing 10% fetal bovine serum at 37°C in the presence of 5% CO_2. Primary human bladder urothelial cells (HBLAK cells, CELLnTEC Advanced Cell Systems, Bern, Switzerland) were cultured in CnT-Prime Epithelial Proliferation (CELLnTec Advanced Cell Systems) media. Human 5637, T24, and HBLAK cells were obtained from men aged 68 years, 45 years, and 80 years, respectively.[72,73] Bladders from control and PTP1B$^{-/-}$mice were dissected under sterile conditions and placed in ice-cold phosphate buffered saline (PBS). Bladders were everted and urothelium was mechanically separated from the detrusor muscle under a dissecting microscope using sterile forceps. Isolated urothelium was cultured to confluency in CnT-Prime Epithelial Proliferation media at 37°C in the presence of 5% CO_2.

METHOD DETAILS

Mouse UTI model—Female mice aged 6–8 weeks were infected by transurethral catheterization with 10^7 CFU UTI89 and male mice were infected using the surgical UTI model as published.[16,74] UTI89 is type I-piliated UPEC strain isolated from a patient with cystitis.[75] At the indicated time points after inoculation, mice were anesthetized and sacrificed via cervical dislocation. Urine was collected and organs were aseptically harvested

and UPEC colonies were enumerated by plating serial dilutions. Counts less than nine CFU at any dilution were below the limits of quantification.

Mouse OSI-906 treatment—Female C3H/HeOuJ mice aged 6–8 weeks were treated with one or two doses of vehicle (tartaric acid) or OSI-906 (Selleckchem, Houston, TX, USA) by oral gavage as outlined in the results section. OSI-906 dosing was based on published data.[32]

Mouse glucose tolerance testing and metabolic measurements—PTP1B$^{-/-}$and control mice were fasted 6 h. Intraperitoneal glucose tolerance testing was performed by injecting mice with D-glucose. Blood glucose concentrations were measured at 15, 30, 60, and 90 min post injection.[76] Blood glucose measurements were obtained using the AlphaTrak glucose monitoring system (Abbott Point of Care, Abbott Park, IL, USA). Urinary glucose measurements were assessed by dipstick urinalysis (Chemstrip 2 GP, Roche, Basel, Switzerland). Serum insulin concentrations were measured with the ultra-sensitive mouse insulin ELISA kit (Crystal Chem, Elk Grove Village, IL, USA).

Mouse bladder histopathology and immunostaining—Bladders were fixed in 4% paraformaldehyde then 70% ethanol and processed for paraffin sectioning. Slides were sectioned at 5μm. Sections used for histopathology were stained with hematoxylin and eosin. Four representative sections were evaluated per organ and bladder pathology was scored as previously described.[77] Immunofluorescent staining and immunohistochemistry was performed following published methods.[16,60] Bladders were labeled with a rabbit PTP1B antibody (Sigma-Aldrich, St. Louis, MO, USA), polyclonal goat Upk3 antibody (Santa Cruz Biotechnology, Dallas, TX, USA), Krt5 antibody (BioLegend, San Diego, CA, USA), polyclonal rabbit IRα antibody (Abcam), polyclonal rabbit NF-κB p65 antibody (Abcam), or a rabbit polyclonal RFP/tdTomato antibody (Rockland Immunochemicals Inc., Limerick, PA, USA). Alexa Fluor 488 AffiniPure Donkey Anti-Goat IgG (Jackson ImmunoResearch Laboratories, West Grove, PA, USA) and Cy3 AffiniPure F(ab')$_2$ Fragment Donkey Anti-Rabbit IgG (Jackson ImmunoResearch Laboratories) served as secondary antibodies.

RNA-protein co-detection—*Insr and* Krt5 were co-detected using the RNAscope 2.5 HD Duplex Assay and RNA-Protein Co-detection Ancillary Kit (Advanced Cell Diagnostics, Hayward, CA, USA). Deparaffinized and dehydrated slides were pretreated using the RNAscope Hydrogen Peroxide (10-min), and RNAscope Co-Detection Target Retrieval (20-min) reagents. Basal cells were labeled with a keratin 5 antibody overnight then slides were fixed in 10% formalin (30 min). Slides were treated with Protease Plus reagent (30-min), hybridized with *Insr*-C2 which recognizes exons 3–5 of the *Insr* gene, *Polr2A*-C2 (positive control), or *DapB*-C2 (negative control) probes (2 h, Advanced Cell Diagnostics), amplified using AMPS 1–6, and C2 signal was visualized using the Detect Red reagents (10 min). Following treatment with Co-Detection Blocker (30 min), a goat anti-rabbit-HRP secondary antibody was applied (1 h, Cell Signaling) and keratin 5 was visualized using 3,3-diaminobenzidine tetrahydrochloride (10 min). Slides were counterstained in 50% Gill's Hematoxylin I (Thermo Fisher Scientific, Waltham, MA, USA). Cover slips were applied with VectaMount (Vector Laboratories, Inc., Burlingame, CA, USA). Images were captured

using a Nikon Ti2-E microscope and DS-RI2 camera (Nikon Instruments Inc., Melville, NY, USA).

Electron microscopy—Transmission electron microscopy was performed as previously described.[78,79] Bladders were fixed in 2% glutaraldehyde/PBS, post-fixed in 1% osmium tetroxide, dehydrated in graded ethanol, cleared in propylene oxide, and placed in 1:1 Epon-Araldite:propylene oxide and Epon–Araldite. Palladium-coated copper grids were used to collect 60-nm sections that were stained with uranyl acetate and lead citrate. Images were captured using a Hitachi H-7650 microscope (Hitachi, Chiyoda, Tokyo, Japan).

Capacitance, transepithelial resistance (TER), and permeability measurements—Mice were anesthetized with isoflurane (5% induction, 2% maintenance). Bladders were excised and placed into Ringer's solution (111.2 mM NaCl, 25 mM $NaHCO_3$, 4.8 mM KCl, 2 mM $CaCl_2$, 1.2 mM $MgSO_4$, 1.2 mM KH_2PO_4 and 11.1 mM glucose, bubbled with 95% O_2/5% CO_2, at 37°C). The bladder was cut open along the ventral axis from base to dome, stretched slightly and mounted on a ring insert with a 0.09 cm^2 opening. The ring with the tissue was then mounted between two-halves of an Ussing chamber filled with bubbled Ringer's solution at 37°C. Tissue was allowed to stabilize for 1 h. Capacitance and TER were determined by regularly passing current through Ag–AgCl electrodes in the rear of each half chamber to measure voltage deflection across the tissue. TER was calculated as maximal voltage change divided by current amplitude and multiplied by area (in cm^2). Capacitance was determined from the Resistor-Capacitor (RC) time constant (t, time required to charge the tissue) and resistance. Water and urea permeabilities were determined using isotopic fluxes. [^{3}H] water (1 μCi/mL) and [^{14}C] urea (0.25 μCi/mL) were added to the urothelial side and duplicate samples were taken every 15 min from both hemichambers for 1–1.5 h. Samples were placed into scintillation fluid for counting and diffusive coefficients calculated as:

$$P_D = \Phi\left(\frac{counts}{\sec}\right)/A\left(cm^2\right)\cdot \Delta C\left(\frac{counts}{cm^3}\right)$$

where Φ = tracer flux (increase in basolateral side), A = area of the apical membrane (from capacitance, $1\ \mu F \approx 1\ cm^2$), ΔC = difference in concentrations of isotope across the membrane.

Mouse bladder flow cytometry—Female IRflox and IRKO bladders were harvested 24 h after transurethral UTI. Bladder tissues were minced and dissociated in DMEM/F-12 supplemented with 100 mg/mL Collagenase I and 10 mM HEPES. After enzymatic dissociation, single cell suspensions were incubated with an anti-mouse Fc receptor antibody to block non-specific antibody binding. Cells were then stained with blue-fluorescent reactive dye (L23105, Life Technologies) for 20 min at room temperature to remove dead cells from the analysis. After washing, $1–3 \times 10^6$ cells were stained for cell surface receptors in FACS buffer for 15 min at 4°C with fluorescent monoclonal antibody combinations as previously published (Key Resource table).[80] Stained cells were collected on an LSR II cytofluorometer (BD, Franklin Lakes, NJ) and data analyzed using the Flowjo software

(Treestar, Ashland, TN). Absolute cell numbers were calculated using countBright absolute counting beads (Thermo Fisher).

Gene silencing by RNA interference *in vitro*—Pooled siRNA libraries targeting *INSR*, *PTP1B*, *AKT1*, *NFKB1*, *CDH1*, *CLDN4*, *TJP1*, and a non-targeting pool (negative control) were purchased (ON-TARGETplus SMARTpool, Dharmacon, Lafayette, CO, USA). Primary human urothelial cells were cultured to 95% confluency and transfected with a mixture of siRNA, DharmaFECT transfection reagent (Dharmacon), and culture media per the manufacturer's recommendations. Forty-eight hours after transfection, RNA was isolated from cells for RT-PCR analysis. Seventy-two hours after transfection, transfected cells were used for UPEC infection assays, drug studies, or permeability assays outlined below.

UPEC attachment and invasion assays—Confluent human urothelial cells were cultured in 24 well plates and transfected with siRNA or treated with the indicated compounds prior to bacterial challenge. Isolated murine urothelial cells were cultured in 96 well plates. Cells were infected with 1 or 10 multiplicity of infection UTI89 when indicated. UPEC attachment and invasion assays were performed as described.[60,61]

***In vitro* permeability and UPEC translocation assay—**Human urothelial cells were cultured on 0.4-μm pore-size (FITC-dextran experiments) or 3-μm pore-size (UPEC experiments) permeable transwell membranes in 24 well plates with the apical chamber containing 200 μL of culture media and the basal chamber containing 700 μL of culture media. Cells were transfected with siRNA pools or treated with OSI-906 (1 μM) for 16 h. Low molecular weight FITC-conjugated dextran (3000–5000 Da, 20 μg/mL, Sigma-Aldrich) or 10 MOI UTI89 were added to the apical cell chamber. Dextran permeability was quantified by measuring the mean fluorescence intensity of the FITC-conjugated detected in the basal chamber using a CLARIOstar *Plus* microplate reader with an excitation of 485 nm and excitation of 535 nm (BMG Labtech, Ortenberg, Germany). Results were plotted showing fold change by dividing the fluorescence measurements in basal chamber medium compared to basal chamber medium collected from control wells where FITC-dextran was not added to the apical chamber. UPEC was enumerated in the basal chamber culture medium by serially diluting a sample of culture medium 3 h after UPEC challenge and plating the dilutions on LB-agar plates.

NF-κB reporter—Human urothelial cells were grown to near confluency and co-transfected with a firefly luciferase NF-κB reporter plasmid pGL4.32 [luc2P/NF-κB-RE/Hygro] (100 ng, Promega, Madison, WI, USA), pRL-CMV Renilla luciferase plasmid (10ng, Promega), and *INSR* or *AKT1* siRNA pools using Lipofectamine 2000. Seventy-two hours after transfection, cells were infected with UTI89. Additionally, cells were transfected with NF-κB reporter and pRL-CMV Renilla plasmids and treated with OSI-906 (1 μM) overnight 48 h after transfection. Seventy-two hours after transfection, cells were treated with OSI-906 (1 μM) overnight and then infected with UTI89. Luciferase activity was measured on a Veritas Microplate Luminometer (Turner BioSystems, Sunnyvale, CA, USA) using Dual-Glo Luciferase Assay Kit according to manufacturer's protocol (Promega).

Chromatin immunoprecipitation (ChIP)—ChIP was performed using SimpleChIP Enzymatic Chromatin IP Kit with magnetic beads per manufacturer's instructions (Cell Signaling). Human urothelial cells were cultured in 15 cm dishes to confluence and incubated with vehicle or OSI-906 (1 μM) for 16 h. Cells were then stimulated with 1 MOI UTI89 for 3 h. Chromatin was prepared according to kit instructions. Immunoprecipitation reactions included a negative control rabbit IgG and a positive control histone H3 and immunoprecipitation was performed using an anti-P65 antibody (Cell Signaling). Following ChIP, PCR reactions were performed with primers targeting P65 peaks for antimicrobial peptide and barrier genes identified using ChIP-seq data from the encyclopedia of DNA elements project (Table S5).[81] Results are expressed as percent precipitated DNA compared to total input, and calculated as follows:

$$\%\ \text{Input} = \frac{100}{2^{(C_T[\text{ChIP}] - (C_T[\ [\text{Input}] - log_2(\text{Input Dilution Factor}))}}$$

RNA isolation and real-time PCR—RNA was isolated using RNeasy Plus Mini Kit (Qiagen, Hilden, Germany) from frozen mouse tissue or cell lysates following manufacturer's instructions. RNA from exfoliated human urothelial cells was isolated using the RNeasy Micro Kit (Qiagen). cDNA was generated using the Verso cDNA synthesis kit (Thermo-Fisher). Quantitative RT-PCR reactions were performed with the 7500 Real-Time PCR System (Applied Biosystems, Carlsbad, CA, USA) as previously described.[82] Each reaction included cDNA, Absolute Blue QPCR SYBR Mix (Thermo-Fisher), and target specific primers (Tables S4 and S5).

Antibacterial response PCR arrays—cDNA was generated using the RT2 First Strand Kit (Qiagen). Mouse Antibacterial Response Arrays (Qiagen) were performed following manufacturer's instructions and analyzed using Qiagen's GeneGlobe Data Analysis Center. Samples were normalized to the average geometric mean of internal controls *Actb*, *B2m*, *Gapdh*, *Gusb*, and *Hsp90ab1*.

Western blot—Western blot was performed as previously described.[60] Antibodies directed against the following targets were used: PTP1B (SigmaAldrich), P-IGF1Rb (Tyr1135/1136)/IRb (Tyr1150/1151) (Cell Signaling), P-AKT (Ser473) (Cell Signaling), NF-κB P-p65 (Ser536) (Cell Signaling), IκBα (Cell Signaling), E-cadherin (Cell Signaling), ZO-1 (Invitrogen), claudin 4 (Fisher), claudin 8 (Invitrogen), and GAPDH (Cell Signaling).

ELISA—Commercial ELISAs quantified urinary concentrations of Lcn 2 (Abcam), RNase 4 (MyBioSource, San Diego, CA, USA), RNase 7 (Hycult Biotech, Plymouth Meeting, PA, USA), and uroplakin 2 (Lifespan Biosciences, Lynnwood, WA, USA). Values were normalized to urine creatinine (Oxford Biomedical Research, Rochester Hills, MI, USA). ELISAs were performed following the manufacturer's instructions.

QUANTIFICATION AND STATISTICAL ANALYSIS

Continuous differences between groups were evaluated for a normal distribution with the D'Agostino-Pearson Omnibus or Shapiro-Wilk normality test, with normality defined as a p

value > 0.05. Comparisons on normally distributed data were performed using a Student's t-test or ANOVA; otherwise, the nonparametric Mann-Whitney U or Kruskal-Wallis tests were used. Data from *in vitro* experiments were normally distributed and are presented as means ± SEM. Differences between groups with a p value < 0.05 were regarded as statistically significant.

Supplementary Material

Refer to Web version on PubMed Central for supplementary material.

ACKNOWLEDGMENTS

We thank Cindy McAllister at the Abigail Wexner Research Institute at Nationwide Children's for preparing the electron microscopy samples and Dr. Rachel Cianciolo at The Ohio State University College of Veterinary Medicine for assistance with capturing images. We also acknowledge Dr. Krista La Perle at The Ohio State University College of Veterinary Medicine for reviewing bladder histopathology. We thank Birong (Rollin) Li for assistance with the mouse UTI model and Isabelle Coburn for collecting human biospecimens. L.S. is supported by the National Institutes of Health Loan Repayment Program. S.L.-P. is supported by The Ohio State University Genentech Veterinary Pathology Fellowship. This work is supported by National Institutes of Health (NIDDK) R01 DK128088, R01 DK114035, and R01 DK115737 (to J.D.S.).

REFERENCES

1. Korbel L, and Spencer JD (2015). Diabetes mellitus and infection: an evaluation of hospital utilization and management costs in the United States. J. Diabet. Complicat. 29, 192–195. 10.1016/j.jdiacomp.2014.11.005.
2. Nitzan O, Elias M, Chazan B, and Saliba W (2015). Urinary tract infections in patients with type 2 diabetes mellitus: review of prevalence, diagnosis, and management. Diabetes Metab. Syndr. Obes. 8, 129–136. 10.2147/DMSO.S51792. [PubMed: 25759592]
3. Geerlings SE (2008). Urinary tract infections in patients with diabetes mellitus: epidemiology, pathogenesis and treatment. Int. J. Antimicrob. Agents 31, S54–S57. 10.1016/j.ijantimicag.2007.07.042. [PubMed: 18054467]
4. Nicolle LE, Friesen D, Harding GK, and Roos LL (1996). Hospitalization for acute pyelonephritis in Manitoba, Canada, during the period from 1989 to 1992; impact of diabetes, pregnancy, and aboriginal origin. Clin. Infect. Dis. 22, 1051–1056. [PubMed: 8783709]
5. Muller LMAJ, Gorter KJ, Hak E, Goudzwaard WL, Schellevis FG, Hoepelman AIM, and Rutten GEHM (2005). Increased risk of common infections in patients with type 1 and type 2 diabetes mellitus. Clin. Infect. Dis. 41, 281–288. 10.1086/431587. [PubMed: 16007521]
6. Liu Y, Mé met S., Saban R., Kong X., Aprikian P., Sokurenko E., Sun TT., and Wu XR. (2015). Dual ligand/receptor interactions activate urothelial defenses against uropathogenic E. coli. Sci. Rep. 5, 16234. 10.1038/srep16234. [PubMed: 26549759]
7. Dalghi MG, Montalbetti N, Carattino MD, and Apodaca G (2020). The Urothelium: Life in a Liquid Environment. Physiol. Rev. 100, 1621–1705. 10.1152/physrev.00041.2019. [PubMed: 32191559]
8. Wu XR, Kong XP, Pellicer A, Kreibich G, and Sun TT (2009). Uroplakins in urothelial biology, function, and disease. Kidney Int. 75, 1153–1165. 10.1038/ki.2009.73. [PubMed: 19340092]
9. Abraham SN, and Miao Y (2015). The nature of immune responses to urinary tract infections. Nat. Rev. Immunol. 15, 655–663. 10.1038/nri3887. [PubMed: 26388331]
10. Becknell B, Schwaderer A, Hains DS, and Spencer JD (2015). Amplifying renal immunity: the role of antimicrobial peptides in pyelonephritis. Nat. Rev. Nephrol. 11, 642–655. 10.1038/nrneph.2015.105. [PubMed: 26149835]
11. Ozer A, Altuntas CZ, Bicer F, Izgi K, Hultgren SJ, Liu G, and Daneshgari F (2015). Impaired cytokine expression, neutrophil infiltration and bacterial clearance in response to urinary tract infection in diabetic mice. Pathog. Dis. 73, ftv002. 10.1093/femspd/ftv002. [PubMed: 25663347]

12. Ozer A, Altuntas CZ, Izgi K, Bicer F, Hultgren SJ, Liu G, and Daneshgari F (2015). Advanced glycation end products facilitate bacterial adherence in urinary tract infection in diabetic mice. Pathog. Dis. 73, ftu004. 10.1093/femspd/ftu004. [PubMed: 25986378]

13. Hanna-Mitchell AT, Ruiz GW, Daneshgari F, Liu G, Apodaca G, and Birder LA (2013). Impact of diabetes mellitus on bladder uroepithelial cells. Am. J. Physiol. Regul. Integr. Comp. Physiol. 304, R84–R93. 10.1152/ajpregu.00129.2012. [PubMed: 23174855]

14. Lee S, Rose'meyer R, McDermott C, Chess-Williams R, and Sellers DJ (2018). Diabetes-induced alterations in urothelium function: Enhanced ATP release and nerve-evoked contractions in the streptozotocin rat bladder. Clin. Exp. Pharmacol. Physiol. 45, 1161–1169. 10.1111/1440-1681.13003. [PubMed: 29935089]

15. Mohanty S, Kamolvit W, Scheffschick A, Bjö rklund A., Tovi J., Espinosa A., Brismar K., Nyströ m T., Schröder JM., Östenson CG., et al. (2022). Diabetes downregulates the antimicrobial peptide psoriasin and increases E. coli burden in the urinary bladder. Nat. Commun. 13, 4983. 10.1038/s41467-022-32636-y. [PubMed: 36127330]

16. Murtha MJ, Eichler T, Bender K, Metheny J, Li B, Schwaderer AL, Mosquera C, James C, Schwartz L, Becknell B, and Spencer JD (2018). Insulin receptor signaling regulates renal collecting duct and intercalated cell antibacterial defenses. J. Clin. Invest. 128, 5634–5646. 10.1172/JCI98595. [PubMed: 30418175]

17. Eichler TE, Becknell B, Easterling RS, Ingraham SE, Cohen DM, Schwaderer AL, Hains DS, Li B, Cohen A, Metheny J, et al. (2016). Insulin and the phosphatidylinositol 3-kinase signaling pathway regulate Ribonuclease 7 expression in the human urinary tract. Kidney Int. 90, 568–579. 10.1016/j.kint.2016.04.025. [PubMed: 27401534]

18. Froy O, Hananel A, Chapnik N, and Madar Z (2007). Differential effect of insulin treatment on decreased levels of beta-defensins and Toll-like receptors in diabetic rats. Mol. Immunol. 44, 796–802. 10.1016/j.molimm.2006.04.009. [PubMed: 16740310]

19. Guo S (2014). Insulin signaling, resistance, and the metabolic syndrome: insights from mouse models into disease mechanisms. J. Endocrinol. 220, T1–T23. 10.1530/JOE-13-0327. [PubMed: 24281010]

20. Boucher J, Kleinridders A, and Kahn CR (2014). Insulin receptor signaling in normal and insulin-resistant states. Cold Spring Harbor Perspect. Biol. 6, a009191. 10.1101/cshperspect.a009191.

21. Taniguchi CM, Emanuelli B, and Kahn CR (2006). Critical nodes in signalling pathways: insights into insulin action. Nat. Rev. Mol. Cell Biol. 7, 85–96. 10.1038/nrm1837. [PubMed: 16493415]

22. Kulkarni RN, Brüning JC, Winnay JN, Postic C, Magnuson MA, and Kahn CR (1999). Tissue-specific knockout of the insulin receptor in pancreatic beta cells creates an insulin secretory defect similar to that in type 2 diabetes. Cell 96, 329–339. [PubMed: 10025399]

23. Michael MD, Kulkarni RN, Postic C, Previs SF, Shulman GI, Magnuson MA, and Kahn CR (2000). Loss of insulin signaling in hepatocytes leads to severe insulin resistance and progressive hepatic dysfunction. Mol. Cell 6, 87–97. [PubMed: 10949030]

24. Brüning M, Michael MD, Peroni OD, Ueki K, Carter N, Kahn BB, and Kahn CR (2002). Adipose tissue selective insulin receptor knockout protects against obesity and obesity-related glucose intolerance. Dev. Cell 3, 25–38. [PubMed: 12110165]

25. Brüning JC, Michael MD, Winnay JN, Hayashi T, Hörsch D, Accili D, Goodyear LJ, and Kahn CR (1998). A muscle-specific insulin receptor knockout exhibits features of the metabolic syndrome of NIDDM without altering glucose tolerance. Mol. Cell 2, 559–569. [PubMed: 9844629]

26. Bunner AE, Chandrasekera PC, and Barnard ND (2014). Knockout mouse models of insulin signaling: Relevance past and future. World J. Diabetes 5, 146–159. 10.4239/wjd.v5.i2.146. [PubMed: 24748928]

27. Hale LJ, and Coward RJM (2013). The insulin receptor and the kidney. Curr. Opin. Nephrol. Hypertens. 22, 100–106. 10.1097/MNH.0b013e32835abb52. [PubMed: 23104093]

28. Andres SF, Santoro MA, Mah AT, Keku JA, Bortvedt AE, Blue RE, and Lund PK (2015). Deletion of intestinal epithelial insulin receptor attenuates high-fat diet-induced elevations in cholesterol and stem, enteroendocrine, and Paneth cell mRNAs. Am. J. Physiol. Gastrointest. Liver Physiol. 308, G100–G111. 10.1152/ajpgi.00287.2014. [PubMed: 25394660]

29. Tsai S, Clemente-Casares X, Zhou AC, Lei H, Ahn JJ, Chan YT, Choi O, Luck H, Woo M, Dunn SE, et al. (2018). Insulin Receptor-Mediated Stimulation Boosts T Cell Immunity during Inflammation and Infection. Cell Metabol. 28, 922–934.e4. 10.1016/j.cmet.2018.08.003.
30. Senokuchi T, Liang CP, Seimon TA, Han S, Matsumoto M, Banks AS, Paik JH, DePinho RA, Accili D, Tabas I, and Tall AR (2008). Forkhead transcription factors (FoxOs) promote apoptosis of insulin-resistant macrophages during cholesterol-induced endoplasmic reticulum stress. Diabetes 57, 2967–2976. 10.2337/db08-0520. [PubMed: 18728232]
31. Ieronymaki E, Theodorakis EM, Lyroni K, Vergadi E, Lagoudaki E, Al-Qahtani A, Aznaourova M, Neofotistou-Themeli E, Eliopoulos AG, Vaporidi K, and Tsatsanis C (2019). Insulin Resistance in Macrophages Alters Their Metabolism and Promotes an M2-Like Phenotype. J. Immunol. 202, 1786–1797. 10.4049/jimmunol.1800065. [PubMed: 30718296]
32. Mulvihill MJ, Cooke A, Rosenfeld-Franklin M, Buck E, Foreman K, Landfair D, O'Connor M, Pirritt C, Sun Y, Yao Y, et al. (2009). Discovery of OSI-906: a selective and orally efficacious dual inhibitor of the IGF-1 receptor and insulin receptor. Future Med. Chem. 1, 1153–1171. 10.4155/fmc.09.89. [PubMed: 21425998]
33. Seely BL, Staubs PA, Reichart DR, Berhanu P, Milarski KL, Saltiel AR, Kusari J, and Olefsky JM (1996). Protein tyrosine phosphatase 1B interacts with the activated insulin receptor. Diabetes 45, 1379–1385. 10.2337/diab.45.10.1379. [PubMed: 8826975]
34. Salmeen A, Andersen JN, Myers MP, Tonks NK, and Barford D (2000). Molecular basis for the dephosphorylation of the activation segment of the insulin receptor by protein tyrosine phosphatase 1B. Mol. Cell 6, 1401–1412. 10.1016/s1097-2765(00)00137-4.
35. Klaman LD, Boss O, Peroni OD, Kim JK, Martino JL, Zabolotny JM, Moghal N, Lubkin M, Kim YB, Sharpe AH, et al. (2000). Increased energy expenditure, decreased adiposity, and tissue-specific insulin sensitivity in protein-tyrosine phosphatase 1B-deficient mice. Mol. Cell Biol. 20, 5479–5489. 10.1128/mcb.20.15.5479-5489.2000. [PubMed: 10891488]
36. Elchebly M, Payette P, Michaliszyn E, Cromlish W, Collins S, Loy AL, Normandin D, Cheng A, Himms-Hagen J, Chan CC, et al. (1999). Increased insulin sensitivity and obesity resistance in mice lacking the protein tyrosine phosphatase-1B gene. Science 283, 1544–1548. 10.1126/science.283.5407.1544. [PubMed: 10066179]
37. Yu Z, Liao J, Chen Y, Zou C, Zhang H, Cheng J, Liu D, Li T, Zhang Q, Li J, et al. (2019). Single-Cell Transcriptomic Map of the Human and Mouse Bladders. J. Am. Soc. Nephrol. 30, 2159–2176. 10.1681/ASN.2019040335. [PubMed: 31462402]
38. Shen TH, Gladoun N, Castillo-Martin M, Bonal D, Domingo-Domenech J, Charytonowicz D, and Cordon-Cardo C (2012). A BAC-based transgenic mouse specifically expresses an inducible Cre in the urothelium. PLoS One 7, e35243. 10.1371/journal.pone.0035243. [PubMed: 22496911]
39. Van Keymeulen A, Rocha AS, Ousset M, Beck B, Bouvencourt G, Rock J, Sharma N, Dekoninck S, and Blanpain C (2011). Distinct stem cells contribute to mammary gland development and maintenance. Nature 479, 189–193. 10.1038/nature10573. [PubMed: 21983963]
40. Liu R, Mathieu C, Berthelet J, Zhang W, Dupret JM, and Rodrigues Lima F (2022). Human Protein Tyrosine Phosphatase 1B (PTP1B): From Structure to Clinical Inhibitor Perspectives. Int. J. Mol. Sci. 23, 7027. 10.3390/ijms23137027. [PubMed: 35806030]
41. Sharma B, Xie L, Yang F, Wang W, Zhou Q, Xiang M, Zhou S, Lv W, Jia Y, Pokhrel L, et al. (2020). Recent advance on PTP1B inhibitors and their biomedical applications. Eur. J. Med. Chem. 199, 112376. 10.1016/j.ejmech.2020.112376. [PubMed: 32416458]
42. Krishnan N, Konidaris KF, Gasser G, and Tonks NK (2018). A potent, selective, and orally bioavailable inhibitor of the protein-tyrosine phosphatase PTP1B improves insulin and leptin signaling in animal models. J. Biol. Chem. 293, 1517–1525. 10.1074/jbc.C117.819110. [PubMed: 29217773]
43. Hussain H, Green IR, Abbas G, Adekenov SM, Hussain W, and Ali I (2019). Protein tyrosine phosphatase 1B (PTP1B) inhibitors as potential anti-diabetes agents: patent review (2015–2018). Expert Opin. Ther. Pat. 29, 689–702. 10.1080/13543776.2019.1655542. [PubMed: 31402706]
44. He RJ, Yu ZH, Zhang RY, and Zhang ZY (2014). Protein tyrosine phosphatases as potential therapeutic targets. Acta Pharmacol. Sin. 35, 1227–1246. 10.1038/aps.2014.80. [PubMed: 25220640]

45. Través PG, Pardo V, Pimentel-Santillana M, González-Rodríguez Á, Mojena M, Rico D, Montenegro Y, Calés C, Martĺ-Sanz P., Valverde AM., and Boscá L. (2014). Pivotal role of protein tyrosine phosphatase 1B (PTP1B) in the macrophage response to pro-inflammatory and anti-inflammatory challenge. Cell Death Dis. 5, e1125. 10.1038/cddis.2014.90. [PubMed: 24625984]
46. Wiede F, Lu KH, Du X, Zeissig MN, Xu R, Goh PK, Xirouchaki CE, Hogarth SJ, Greatorex S, Sek K, et al. (2022). PTP1B Is an Intracellular Checkpoint that Limits T-cell and CAR T-cell Antitumor Immunity. Cancer Discov. 12, 752–773. 10.1158/2159-8290.CD-21-0694. [PubMed: 34794959]
47. Xu X, Wang X, Guo Y, Bai Y, He S, Wang N, Lin Y, Fisher M, Liu Q, and Yao Y (2019). Inhibition of PTP1B Promotes M2 Polarization via MicroRNA-26a/MKP1 Signaling Pathway in Murine Macrophages. Front. Immunol. 10, 1930. 10.3389/fimmu.2019.01930. [PubMed: 31474996]
48. Thaiss CA, Levy M, Grosheva I, Zheng D, Soffer E, Blacher E, Braverman S, Tengeler AC, Barak O, Elazar M, et al. (2018). Hyperglycemia drives intestinal barrier dysfunction and risk for enteric infection. Science 359, 1376–1383. 10.1126/science.aar3318. [PubMed: 29519916]
49. Patrick P, Price TO, Diogo AL, Sheibani N, Banks WA, and Shah GN (2015). Topiramate Protects Pericytes from Glucotoxicity: Role for Mitochondrial CA VA in Cerebromicrovascular Disease in Diabetes. J. Endocrinol. Diabetes 2. 10.15226/2374-6890/2/2/00123.
50. Kuo WT, Zuo L, Odenwald MA, Madha S, Singh G, Gurniak CB, Abraham C, and Turner JR (2021). The Tight Junction Protein ZO-1 Is Dispensable for Barrier Function but Critical for Effective Mucosal Repair. Gastroenterology 161, 1924–1939. 10.1053/j.gastro.2021.08.047. [PubMed: 34478742]
51. van Sloten TT, Sedaghat S, Carnethon MR, Launer LJ, and Stehouwer CDA (2020). Cerebral microvascular complications of type 2 diabetes: stroke, cognitive dysfunction, and depression. Lancet Diabetes Endocrinol. 8, 325–336. 10.1016/S2213-8587(19)30405-X. [PubMed: 32135131]
52. Man MQ, Wakefield JS, Mauro TM, and Elias PM (2022). Alterations in epidermal function in type 2 diabetes: Implications for the management of this disease. J. Diabetes 14, 586–595. 10.1111/1753-0407.13303. [PubMed: 36043448]
53. Wood MW, Breitschwerdt EB, Nordone SK, Linder KE, and Gookin JL (2012). Uropathogenic E. coli promote a paracellular urothelial barrier defect characterized by altered tight junction integrity, epithelial cell sloughing and cytokine release. J. Comp. Pathol. 147, 11–19. 10.1016/j.jcpa.2011.09.005. [PubMed: 22014415]
54. Winer DA, Luck H, Tsai S, and Winer S (2016). The Intestinal Immune System in Obesity and Insulin Resistance. Cell Metabol. 23, 413–426. 10.1016/j.cmet.2016.01.003.
55. Rizk DEE, Padmanabhan RK, Tariq S, Shafiullah M, and Ahmed I (2006). Ultra-structural morphological abnormalities of the urinary bladder in streptozotocin-induced diabetic female rats. Int. UrogynEcol. J. Pelvic Floor Dysfunct. 17, 143–154. 10.1007/s00192-005-1359-5. [PubMed: 16021327]
56. Bassam Elnagar AM, Ibrahim S, Abouelnaga MAM, and Soliman AM (2018). Structural Changes in the Urinary Bladder of Streptozotocin-Induced DiabeticRats and the Possible Protective Role of Insulin. IIUM Medical Journal Malaysia 17. 10.31436/imjm.v17i3.247.
57. Schwaderer AL, Wang H, Kim S, Kline JM, Liang D, Brophy PD, McHugh KM, Tseng GC, Saxena V, Barr-Beare E, et al. (2016). Polymorphisms in alpha-Defensin-Encoding DEFA1A3 Associate with Urinary Tract Infection Risk in Children with Vesicoureteral Reflux. J. Am. Soc. Nephrol. 27, 3175–3186. 10.1681/ASN.2015060700. [PubMed: 26940096]
58. Houamel D, Ducrot N, Lefebvre T, Daher R, Moulouel B, Sari MA, Letteron P, Lyoumi S, Millot S, Tourret J, et al. (2016). Hepcidin as a Major Component of Renal Antibacterial Defenses against Uropathogenic Escherichia coli. J. Am. Soc. Nephrol. 27, 835–846. 10.1681/ASN.2014101035. [PubMed: 26293821]
59. Steigedal M, Marstad A, Haug M, Damås JK, Strong RK, Roberts PL, Himpsl SD, Stapleton A, Hooton TM, Mobley HLT, et al. (2014). Lipocalin 2 imparts selective pressure on bacterial growth in the bladder and is elevated in women with urinary tract infection. J. Immunol. 193, 6081–6089. 10.4049/jimmunol.1401528. [PubMed: 25398327]

60. Bender K, Schwartz LL, Cohen A, Vasquez CM, Murtha MJ, Eichler T, Thomas JP, Jackson A, and Spencer JD (2021). Expression and function of human ribonuclease 4 in the kidney and urinary tract. Am. J. Physiol. Ren. Physiol. 320, F972–F983. 10.1152/aj-prenal.00592.2020.
61. Eichler T, Bender K, Murtha MJ, Schwartz L, Metheny J, Solden L, Jaggers RM, Bailey MT, Gupta S, Mosquera C, et al. (2019). Ribonuclease 7 Shields the Kidney and Bladder from Invasive Uropathogenic Escherichia coli Infection. J. Am. Soc. Nephrol. 30, 1385–1397. 10.1681/ASN.2018090929. [PubMed: 31239387]
62. Chromek M, Slamová Z, Bergman P, Kovács L, Podracká L, Ehrén I, Hökfelt T, Gudmundsson GH, Gallo RL, Agerberth B, and Brauner A (2006). The antimicrobial peptide cathelicidin protects the urinary tract against invasive bacterial infection. Nat. Med. 12, 636–641. [PubMed: 16751768]
63. Brauner H, Lüthje P, Grünler J, EκBerg NR, Dallner G, Brismar K, and Brauner A (2014). Markers of innate immune activity in patients with type 1 and type 2 diabetes mellitus and the effect of the anti-oxidant coenzyme Q10 on inflammatory activity. Clin. Exp. Immunol. 177, 478–482. 10.1111/cei.12316. [PubMed: 24593795]
64. Liu C, Tate T, Batourina E, Truschel ST, Potter S, Adam M, Xiang T, Picard M, Reiley M, Schneider K, et al. (2019). Pparg promotes differentiation and regulates mitochondrial gene expression in bladder epithelial cells. Nat. Commun. 10, 4589. 10.1038/s41467-019-12332-0. [PubMed: 31597917]
65. Kane LP, Shapiro VS, Stokoe D, and Weiss A (1999). Induction of NF-kappaB by the Akt/PKB kinase. Curr. Biol. 9, 601–604. 10.1016/s0960-9822(99)80265-6. [PubMed: 10359702]
66. Bai D, Ueno L, and Vogt PK (2009). Akt-mediated regulation of NFkappaB and the essentialness of NFkappaB for the oncogenicity of PI3K and Akt. Int. J. Cancer 125, 2863–2870. 10.1002/ijc.24748. [PubMed: 19609947]
67. Hopkins WJ, Gendron-Fitzpatrick A, Balish E, and Uehling DT (1998). Time course and host responses to Escherichia coli urinary tract infection in genetically distinct mouse strains. Infect. Immun. 66, 2798–2802. [PubMed: 9596750]
68. O'Brien VP, Dorsey DA, Hannan TJ, and Hultgren SJ (2018). Host restriction of Escherichia coli recurrent urinary tract infection occurs in a bacterial strain-specific manner. PLoS Pathog. 14, e1007457. 10.1371/journal.ppat.1007457. [PubMed: 30543708]
69. Hultgren SJ, Schwan WR, Schaeffer AJ, and Duncan JL (1986). Regulation of production of type 1 pili among urinary tract isolates of Escherichia coli. Infect. Immun. 53, 613–620. 10.1128/iai.54.3.613-620.1986.
70. Madisen L, Zwingman TA, Sunkin SM, Oh SW, Zariwala HA, Gu H, Ng LL, Palmiter RD, Hawrylycz MJ, Jones AR, et al. (2010). A robust and high-throughput Cre reporting and characterization system for the whole mouse brain. Nat. Neurosci. 13, 133–140. 10.1038/nn.2467. [PubMed: 20023653]
71. Sohal DS, Nghiem M, Crackower MA, Witt SA, Kimball TR, Tymitz KM, Penninger JM, and Molkentin JD (2001). Temporally regulated and tissue-specific gene manipulations in the adult and embryonic heart using a tamoxifen-inducible Cre protein. Circ. Res. 89, 20–25. 10.1161/hh1301.092687. [PubMed: 11440973]
72. Hoffmann MJ, Koutsogiannouli E, Skowron MA, Pinkerneil M, Niegisch G, Brandt A, Stepanow S, Rieder H, and Schulz WA (2016). The New Immortalized Uroepithelial Cell Line HBLAK Contains Defined Genetic Aberrations Typical of Early Stage Urothelial Tumors. Bladder Cancer 2, 449–463. 10.3233/BLC-160065. [PubMed: 28035326]
73. Horsley H, Dharmasena D, Malone-Lee J, and Rohn JL (2018). A urine-dependent human urothelial organoid offers a potential alternative to rodent models of infection. Sci. Rep. 8, 1238. 10.1038/s41598-018-19690-7. [PubMed: 29352171]
74. Olson PD, McLellan LK, Hreha TN, Liu A, Briden KE, Hruska KA, and Hunstad DA (2018). Androgen exposure potentiates formation of intratubular communities and renal abscesses by Escherichia coli. Kidney Int. 94, 502–513. 10.1016/j.kint.2018.04.023. [PubMed: 30041870]
75. Mulvey MA, Schilling JD, and Hultgren SJ (2001). Establishment of a persistent Escherichia coli reservoir during the acute phase of a bladder infection. Infect. Immun. 69, 4572–4579. 10.1128/IAI.69.7.4572-4579.2001. [PubMed: 11402001]
76. https://www.diacomp.org/shared/document.aspx?id=11&docType=Protocol.

77. Bjorling DE, Wang ZY, Boldon K, and Bushman W (2008). Bacterial cystitis is accompanied by increased peripheral thermal sensitivity in mice. J. Urol. 179, 759–763. 10.1016/j.juro.2007.09.024. [PubMed: 18082197]

78. Carpenter AR, Becknell MB, Ching CB, Cuaresma EJ, Chen X, Hains DS, and McHugh KM (2016). Uroplakin 1b is critical in urinary tract development and urothelial differentiation and homeostasis. Kidney Int. 89, 612–624. 10.1016/j.kint.2015.11.017. [PubMed: 26880456]

79. Jackson AR, Li B, Cohen SH, Ching CB, McHugh KM, and Becknell B (2018). The uroplakin plaque promotes renal structural integrity during congenital and acquired urinary tract obstruction. Am. J. Physiol. Ren. Physiol. 315, F1019–F1031. 10.1152/ajprenal.00173.2018.

80. Schwartz L, Bochter MS, Simoni A, Bender K, de Dios Ruiz Rosado J., Cotzomi-Ortega I., Sanchez-Zamora YI., Becknell B., Linn S., Li B., et al. (2023). Repurposing HDAC inhibitors to enhance ribonuclease 4 and 7 expression and reduce urinary tract infection. Proc. Natl. Acad. Sci. USA 120, e2213363120. 10.1073/pnas.2213363120. [PubMed: 36652479]

81. Rosenbloom KR, Sloan CA, Malladi VS, Dreszer TR, Learned K, Kirkup VM, Wong MC, Maddren M, Fang R, Heitner SG, et al. (2013). ENCODE data in the UCSC Genome Browser: year 5 update. Nucleic Acids Res. 41, D56–D63. 10.1093/nar/gks1172. [PubMed: 23193274]

82. Spencer JD, Schwaderer AL, Dirosario JD, McHugh KM, McGillivary G, Justice SS, Carpenter AR, Baker PB, Harder J, and Hains DS (2011). Ribonuclease 7 is a potent antimicrobial peptide within the human urinary tract. Kidney Int. 80, 174–180. 10.1038/ki.2011.109. [PubMed: 21525852]

Highlights

- Lowered insulin receptor signaling in suprabasal bladder urothelial cells elevates UTI risk
- Loss of urothelial insulin receptor signaling suppresses NF-κB immune responses
- Insulin receptor governs bladder barrier integrity and antimicrobial peptides through NF-κB
- Augmenting insulin receptor signaling reduces UTI susceptibility

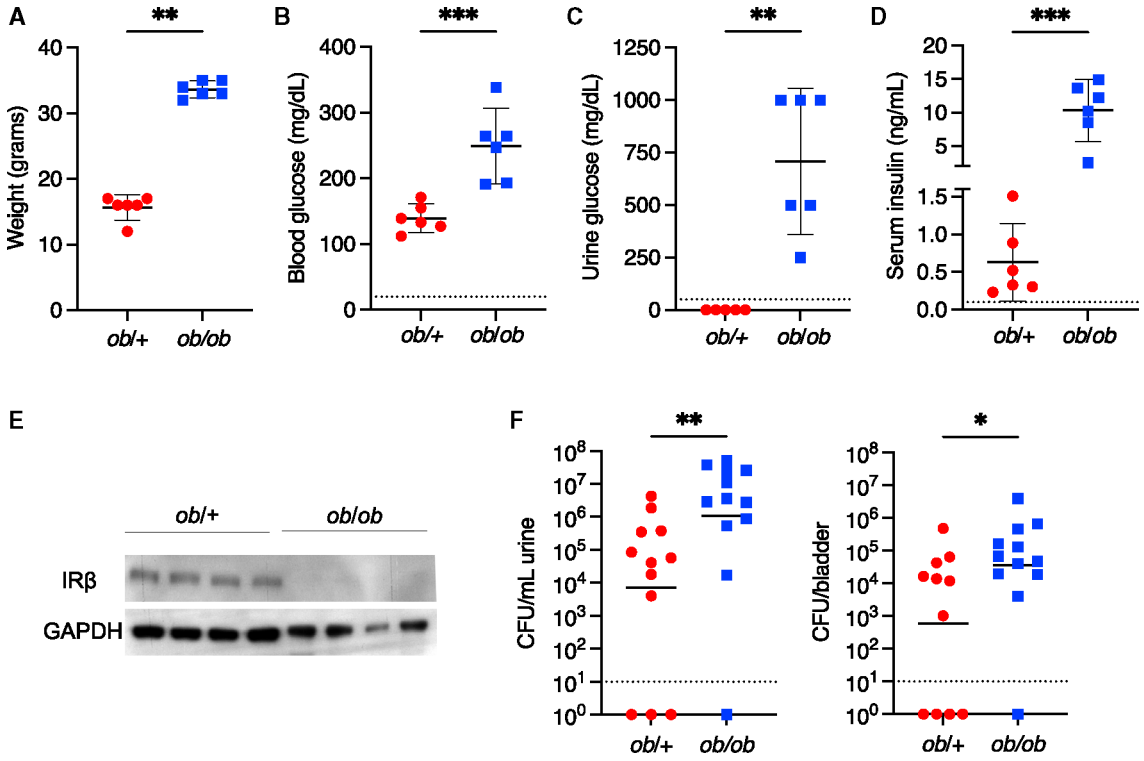

Figure 1. Type 2 diabetes mellitus increases susceptibility to UPEC

(A–D) Body weight (A), blood glucose (B), urine glucose (C), and serum insulin concentrations (D) measured in 7-week-old female non-diabetic *ob*/+ and diabetic *ob*/*ob* mice. Graphs show the mean values and SEM.

(E)Representative western blots probed for IRb and GAPDH in bladders from *ob*/+ and *ob*/*ob* mice.

(F) Urine and bladder UPEC burden enumerated 24 h after transurethral UTI. Urine (left) and bladder (right) UTI89 burden were combined from three independent experiments. The horizontal line indicates the geometric mean of each group.

Each data point or lane represents a sample isolated from an individual animal. The dotted line represents the limits of detection. Asterisks indicate significant p values for the indicated pairwise comparison (Mann-Whitney U test). *$p < 0.05$, **$p < 0.01$, and ***$p < 0.001$.

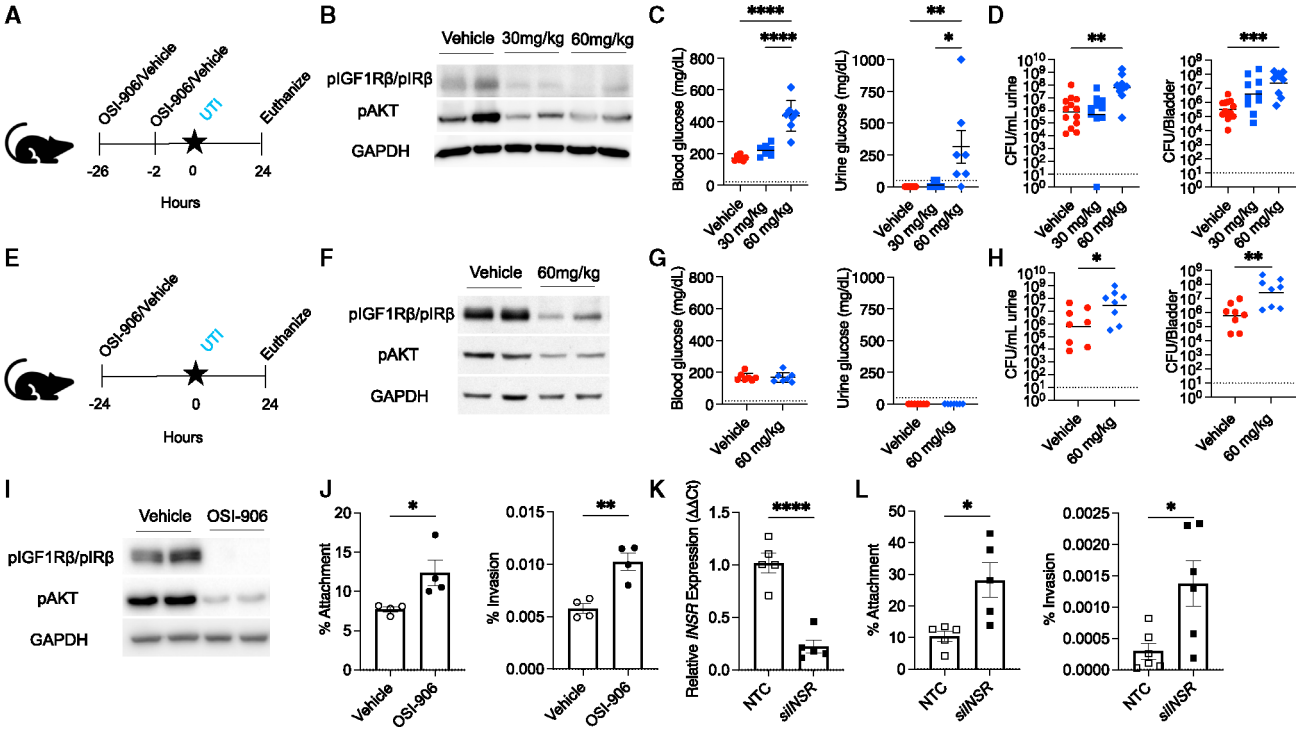

Figure 2. Systemic IR inhibition promotes UTI

(A and E) Schematic showing how female C3H/HeOuJ mice were treated orally with OSI-906 or vehicle before transurethral UTI.

(B and F) Representative western blots probed for pIGF1Rb (Tyr1131)/pIRb (Tyr1146), pAKT (Ser473), and GAPDH using bladders collected from mice treated with vehicle or OSI-906 at the indicated dosages.

(C and G) Blood glucose (left) and urinary glucose (right) concentrations in mice treated with vehicle or OSI-906 at the indicated concentrations. Graphs show the mean glucose concentration and SEM measured at the time of infection. The dotted line represents the limits of detection.

(D and H) Urine (left) and bladder (right) UTI89 burden enumerated 24 h after infection in vehicle- and OSI-906-treated mice. The horizontal line indicates the geometric mean. The dotted line represents the limits of UPEC detection.

(C, D, and H) Asterisks indicate statistical significance as determined by Kruskal-Wallis (C and D) or Mann-Whitney U test (H). (B–D and F–H) Each lane or data point represents a sample isolated from an individual mouse.

(I and J) Human urothelial cells were pretreated with vehicle or OSI-906 (1 μM) for 16 h.

(I) Western blot showing inhibition of IR signaling with OSI-906 treatment.

(J) Vehicleor OSI-906-treated cells were challenged with one multiplicity of infection (MOI) UTI89. Shown are the percentages of bacteria attaching to the cellular surface (left) or invading the cells (right).

(K and L) Human urothelial cells were transfected with an *INSR* or a non-targeting control (NTC) control siRNA pool.

(K) Real-time PCR confirmed *INSR* knockdown.

(L) Transfected cells were challenged with 10 MOI UTI89. Shown are the percentages of bacteria adhering to the cellular surface (left) or invading the cells (right). Graphs show the mean and SEM.

(J–L) Results are from 4–6 independent experiments performed in duplicate.

Asterisks denote significant p values for the pairwise comparison (Student's t test). *$p < 0.05$, **$p < 0.01$, ***$p < 0.001$, and ****$p < 0.0001$. Additionally, refer to Figures S2–S4.

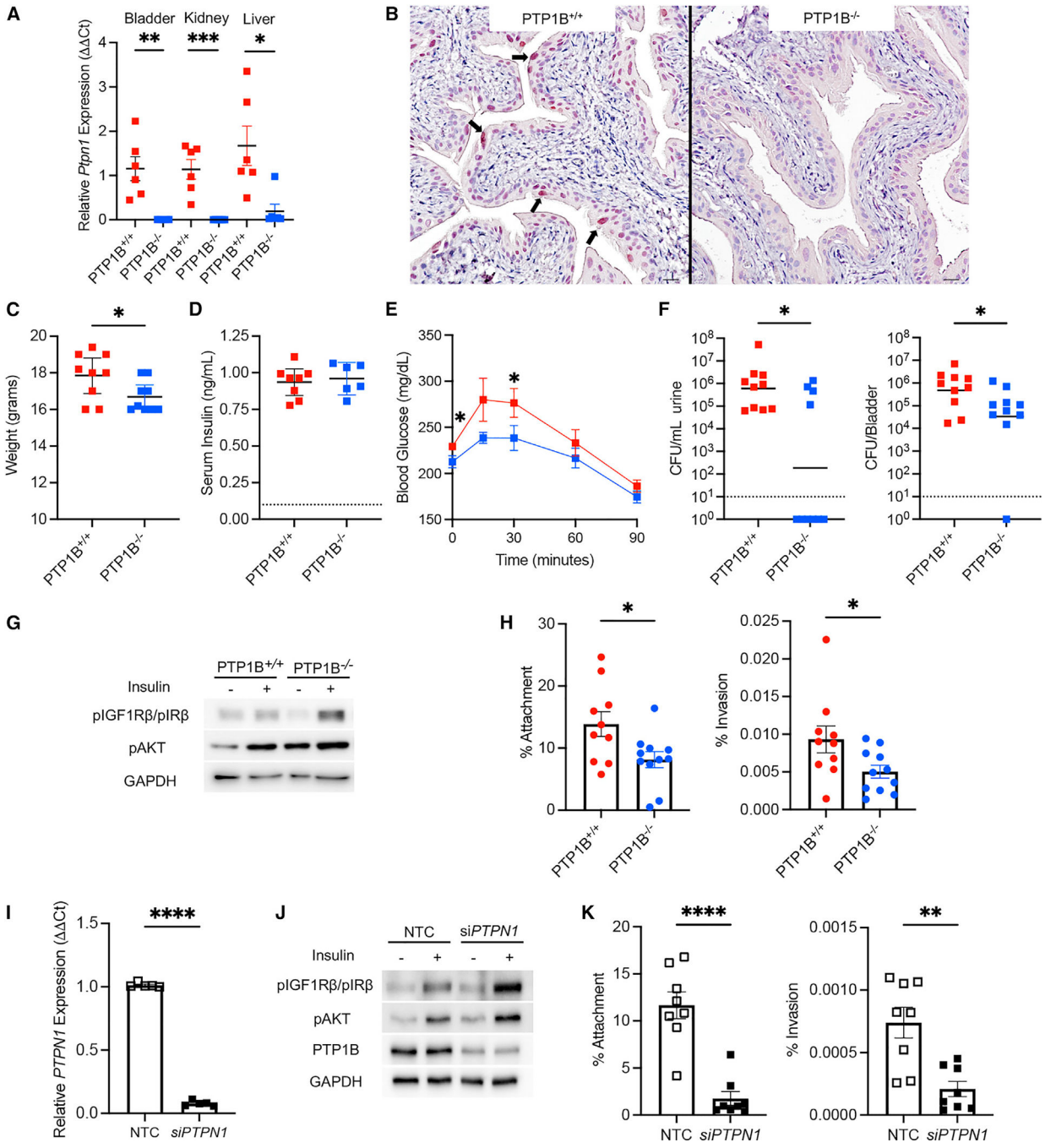

Figure 3. IR activation reduces UTI susceptibility

(A) Relative *Ptpn1* mRNA expression in tissues collected from 6to 8-week-old female *PTP1B*$^{+/+}$ and *PTP1B*$^{-/-}$ mice.

(B) Bladder PTP1B protein expression (brown, arrows). PTP1B was not detected in *PTP1B*$^{-/-}$ mice. Scale bars denote 50 μm.

(C–E) Body weight (C), serum insulin concentrations (D), and blood glucose concentrations following intraperitoneal glucose tolerance testing (E) in female *PTP1B*$^{+/+}$ and *PTP1B*$^{-/-}$ mice. Data are presented as the mean values and SEM.

(F) Urine (left) and bladder (right) UTI89 burden enumerated 24 h after transurethral infection in female *PTP1B*$^{+/+}$ and *PTP1B*$^{-/-}$ mice. The horizontal line indicates the geometric mean of each group. The dotted line represents the limits of UPEC detection as defined in the STAR Methods.

(A and C–F) Each data point represents a sample isolated from an individual animal.

(G and H) Urothelium was isolated from bladders of *PTP1B*$^{+/+}$ and *PTP1B*$^{-/-}$ mice and cultured.

(G) Representative western blots probed for pIGF1Rβ (Tyr1131)/pIRβ (Tyr1146), pAKT (Ser473), and GAPDH in cultured urothelium treated with insulin (100 nM) or vehicle for 30 min.

(H) Urothelial cells were challenged with 10 MOI UTI89. Shown are the percentages of UPEC attaching to the urothelial surface (left) or invading the cells (right). Graphs show the mean number of UPEC colonies enumerated from a unique mouse bladder and SEM.

(I–K) Primary human urothelial cells were transfected with a *PTPN1* or a NTC control siRNA pool and challenged with UPEC.

(I)Real-time PCR confirmed *PTPN1* knockdown.

(J)Representative western blots probed for pIGF1Rβ/pIRβ, pAKT, PTP1B, and GAPDH in cells treated with insulin (100 nM) or vehicle for 30 min.

(K) Transfected human urothelial cells were challenged with 10 MOI UTI89. Shown are the percentages of bacteria attaching to the cellular surface (left) or invading the cells (right). Graphs show the mean and SEM. Results are from eight independent experiments performed in duplicate. Asterisks indicate statistical significance as determined by a Student's t test (A, C–E, H, I, and K) or Mann-Whitney U test (F). *$p < 0.05$, **$p < 0.01$, ***$p < 0.001$, and ****$p < 0.0001$. Additionally, refer to Figures S5 and S6.

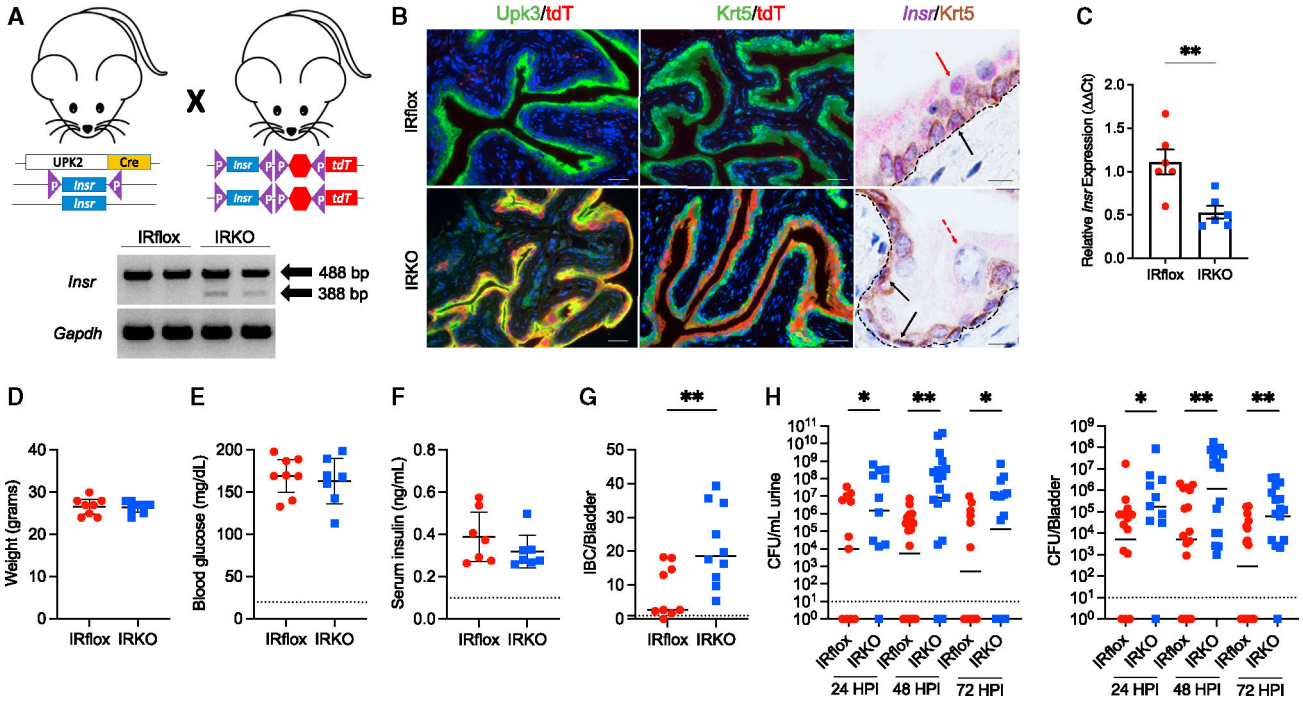

Figure 4. IR deletion in superficial and intermediate urothelial cells increases UPEC susceptibility

(A) Top: schematic of the breeding strategy used to delete *Insr* using Uroplakin 2 (Upk2)-iCre transgenic mice. Bottom: representative PCR gel showing a 488-bp product indicative of the IR floxed allele in bladders of IRflox mice. In IRKO bladders, PCR shows the 488-bp product and a smaller 388-bp product. The 388-bp product confirms *Insr* exon 4 deletion, and the 488-bp product is attributed to other bladder cell types not targeted by Cre recombinase. *Gapdh* is a loading control. Each lane shows results from a separate mouse.

(B) Left and center: representative immunofluorescent staining of murine bladders confirms tdT expression in bladders of Upk2-iCre IRKO mice (tdT, red, left and center columns). tdT expression is restricted to uroplakin 3-expressing superficial and intermediate cells (Upk3, green, left columns) but not basal keratin 5 expressing cells (Krt5, green, center columns). Nuclei are labeled blue. Scale bars denote 50 μm. Right: representative *in situ* hybridization images show *Insr* expression (pink) in apical urothelial cells (red arrow) and basal Krt5 urothelial cells (brown, black arrow) in IRflox mice (top). In IRKO mice (bottom), *Insr* is detected in basal Krt5 urothelial cells (brown, black arrow) but absent in apical urothelial cells (dashed red arrow). Scale bars represent 10 μm. The dashed black line marks the urothelial and stromal interface. Immunofluorescent staining and *in situ* hybridization were completed on 4 bladders from unique IRflox and IRKO mice.

(C) Relative *Insr* transcript expression in urothelium of IRflox and Upk2-iCre IRKO mice. Asterisks show significance between genotypes (n = 6 mice/genotype, unpaired t test).

(D–F) Body weight (D), blood glucose (E), and serum insulin concentrations (F) measured in IRflox and Upk2-iCre IRKO mice. Graphs show the mean values and SEM. The dotted line represents the limits of detection.

(G) Bladder intracellular bacterial communities (IBCs) enumerated 6 h after transurethral infection in female IRflox and Upk2-iCre IRKO mice. The horizontal line shows the mean of each group. The dotted line represents the limits of detection.
(H) Urine (left) and bladder (right) UTI89 burden 24 h post infection (HPI) in female IRflox and Upk2-iCre IRKO mice. The horizontal line shows the geometric mean of each group. Each point denotes a sample isolated from a unique mouse. The dotted line represents the limits of UPEC detection.
(G and H) Asterisks identify significant p values for the indicated pairwise comparisons (Mann-Whitney U test). *$p < 0.05$ and **$p < 0.01$. Additionally, refer to Figures S7–S9.

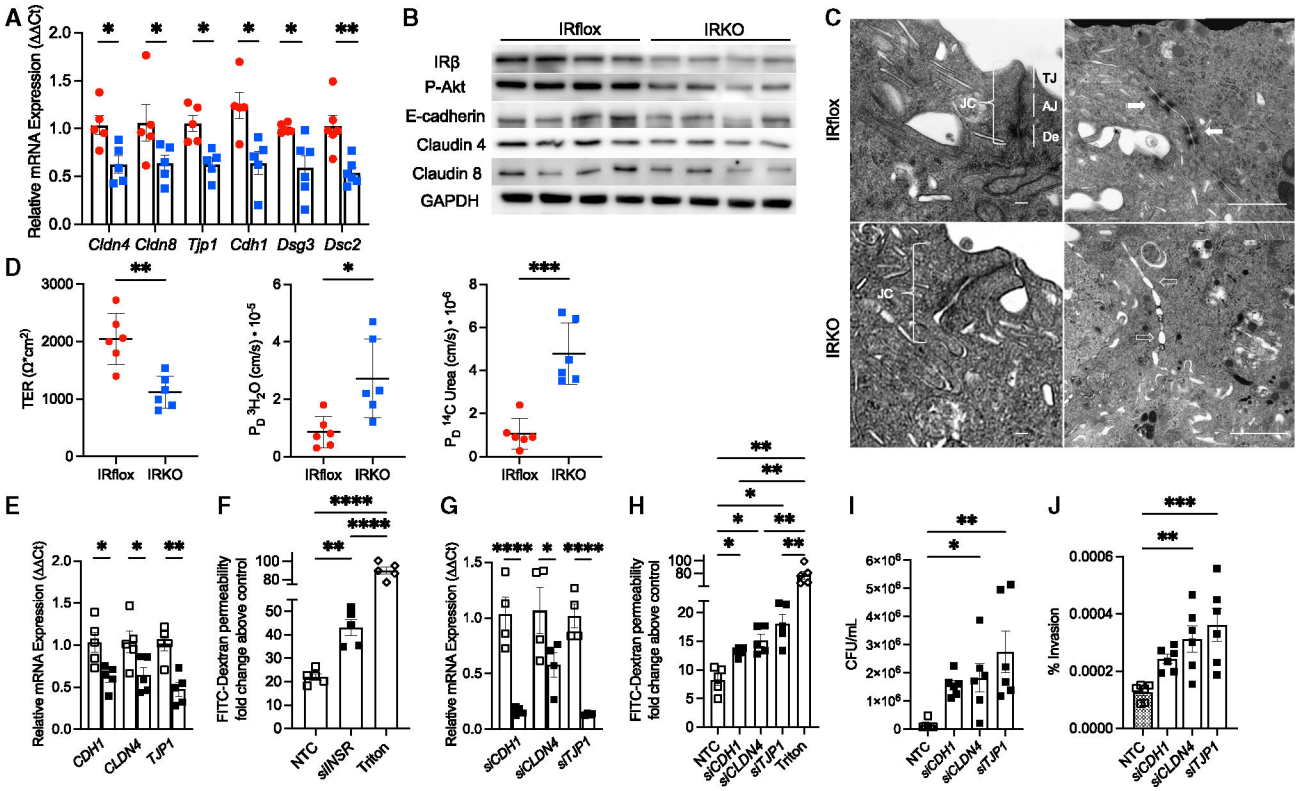

Figure 5. IR deletion in suprabasal urothelial cells compromises the urothelial barrier

(A)Expression of urothelial barrier genes in non-infected bladder urothelium of IRflox (red circles) and Upk2-iCre IRKO mice (blue squares). Asterisks show significance between genotypes (n = 4–5 mice/genotype, unpaired t test).

(B) Representative western blots using non-infected urothelium from IRflox and Upk2-iCre IRKO mice. Each lane depicts protein expression from a separate mouse.

(C) Representative high-power (left column) and low-power (right column) transmission electron micrographs of non-infected IRflox and Upk2-iCre IRKO bladders. Left column: the brackets mark the urothelial junctional complex (JC), which is composed of tight junctions (TJs), the sub-adjacent adherens junction (AJ), and desmosomes (De). Right: The solid arrows denote intact cellular junctions (top). The open arrows mark increased space between cellular junctions (bottom).

(D) Bladder transepithelial resistance (TER; left) and permeability diffusive coefficients (P_D) for water (center) and urea (right) in non-infected IRflox and Upk2-iCre IRKO bladders. Graphs show the mean and standard deviation. Asterisks identify significance between genotypes (n = 6 mice/genotype, unpaired t test).

(E) Human urothelial cells were transfected with an *INSR* (closed squares) or an NTC siRNA pool (open squares). Real-time PCR shows suppressed barrier gene expression with *INSR* silencing. Graphs show the mean and SEM from five independent experiments performed in duplicate (n = 5). Asterisks denote significant p values for the pairwise comparison (t test).

(F) Human urothelial cells were cultured on Transwell inserts and transfected with an *INSR* (closed squares) or an NTC siRNA pool (open squares). Low-molecular-weight FITC-

conjugated dextran was added to the apical chamber culture medium, and fluorescence was measured in the basal chamber medium 180 min later. The addition of Triton X-100 served as a positive control. The graph shows the fold increase in fluorescence measurements in basal chamber medium compared with basal chamber medium collected from cells where FITC-dextran was not added to the apical chamber. Results are from five independent experiments performed in duplicate (n = 5). Asterisks denote significant p values for the indicated comparisons (ANOVA).

(G–J) Human urothelial cells were cultured on Transwell inserts and transfected with *CDH1*, *CLDN4*, *TJP1*, or NTC siRNA pools.

(G) Real-time PCR confirms suppressed target gene expression (closed squares) compared with NTC cells (open squares). Graphs show the mean and SEM from four independent experiments performed in duplicate (n = 4). Asterisks denote significant p values for the pairwise comparison (t test).

(H) FITC-conjugated dextran was added to the apical culture medium of siRNA-transfected cells, and fluorescence was measured in the basal chamber medium 180 min later. The addition of Triton X-100 served as a positive control. The graph shows the fold increase in fluorescence measurements in medium from the basal chamber compared with basal chamber medium collected from cells where FITC-dextran was not added to the apical chamber. Results are from five independent experiments performed in duplicate (n = 5).

(I) UPEC was added to the apical chamber of siRNA-transfected cells and enumerated in the basal chamber medium 180 min later. Graphs show the mean number of recovered colony-forming units (CFUs) and SEM. Results are from 6 independent experiments performed in duplicate (n = 6).

(J) Three days after siRNA transfection, cells were challenged with 10 MOI UPEC. Shown are the percentages of invading bacteria. Graphs show the mean and SEM. Results are from six independent experiments performed in triplicate (n = 6).

(H–J) Asterisks denote significant *p* values as determined by one-way ANOVA. *p < 0.05, **p < 0.01, ***p < 0.001, and ****p < 0.0001.

Additionally, refer to Figures S10–S12 and Table S1.

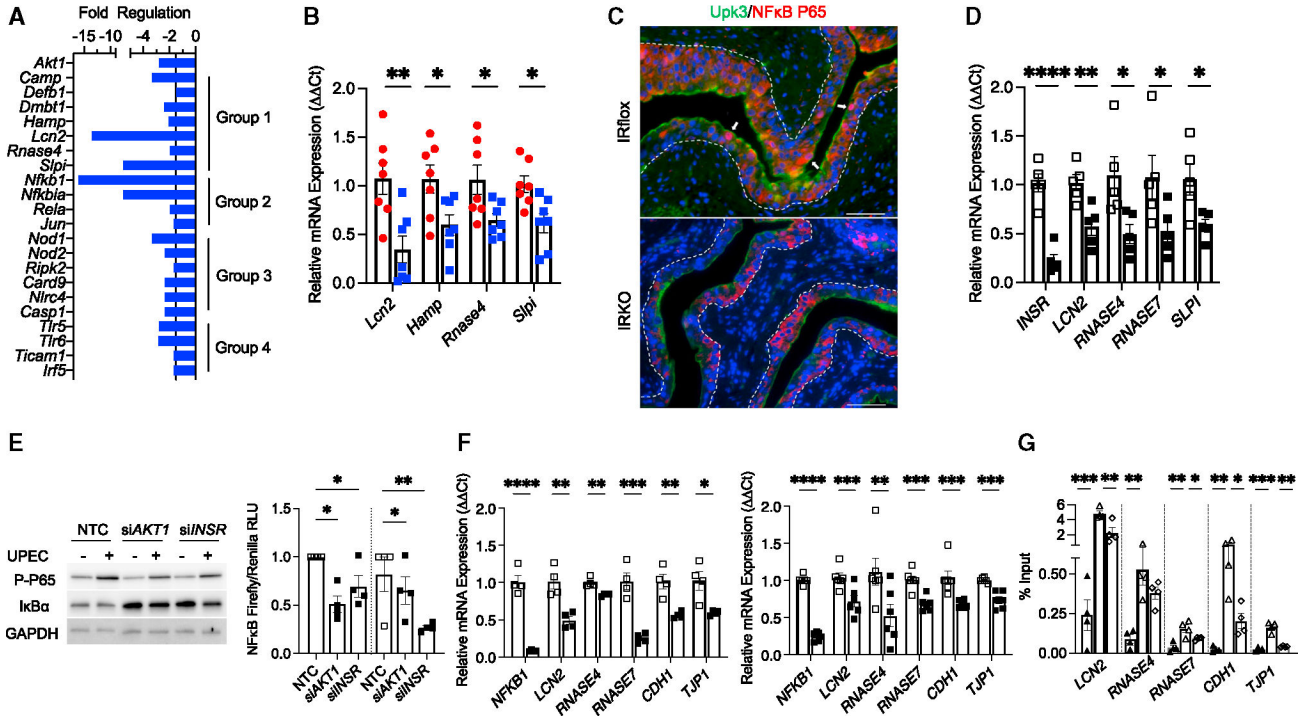

Figure 6. IR deletion suppresses urothelial immune defenses

(A) Downregulated genes (≥1.5-fold regulation, $p < 0.05$) in urothelium isolated from non-infected IRflox and Upk2-iCre IRKO mouse bladders (n = 4 samples/genotype).

(B) Relative transcript expression of antimicrobial peptides in urothelium isolated from UPEC-infected bladders of IRflox (red circles) and Upk2-iCre IRKO mice (blue squares) 24 h after UTI. Asterisks denote significance between genotypes (n = 7 mice/genotype, t test).

(C) Representative immunofluorescent staining of UPEC-infected bladders 24 h after infection from IRflox and Upk2-iCre mice. Upk3 is labeled green, NF-κB P65 red, and nuclei blue. Arrows denote nuclear NF-κB P65 expression in apical cells of IRflox bladders that is largely absent in IRKO bladders. The dashed white line marks the urothelial and stromal interface. Scale bars denote 50 μm. Staining was completed on 4 bladders per genotype.

(D) Human urothelial cells were transfected with NTC or *INSR* siRNA pools. Real-time PCR shows suppressed antimicrobial peptide gene expression (closed squares) compared with NTC cells (open squares). Graphs show the mean and SEM from five independent experiments performed in duplicate (n = 5).

(E) Left: primary human urothelial cells were transfected with siRNA targeting *AKT1*, *INSR*, or NTC and then challenged with 10 MOI UPEC for 1 h. Shown are representative western blots probed for IκBα, P-P65 NF-κβ (Ser536), and GAPDH. Right: human urothelial cells were co-transfected with an NF-κB luciferase construct as well as control (NTC), *INSR*, or *AKT1* siRNA pools. Luciferase activity was measured in non-infected cells and cells infected with UPEC for 60 min. Graphs show the mean and SEM firefly luciferase relative light units (RLUs) normalized to *Renilla*. Results are from four independent experiments performed in sextuplicate (n = 4). Asterisks denote significant p values as determined by one-way ANOVA.

(F) Human urothelial cells were transfected with an *NFKB1* (closed squares) or an NTC control siRNA pool (open squares). Shown is relative transcript expression in non-infected cells (left) or cells infected with UTI89 for 1 h (right). Graphs show the mean expression and SEM from four or six independent experiments performed in duplicate (n = 4–6).
(G) Primary human urothelial cells were pretreated with vehicle (triangles) or OSI-906 (open diamonds). ChIP was performed using non-infected (closed triangles) and UPEC-challenged urothelial cells (open triangles and diamonds). Binding of P65 NF-κB to gene promoters was assessed by real-time PCR with immunoprecipitated DNA using primers specific to promoter regions of the respective genes. Graphs show the mean and SEM of precipitated DNA compared with total input as calculated in the STAR Methods. Results are from 4 independent experiments. Asterisks denote significant p values for the pairwise comparison (E, t test; F, one-way ANOVA). *$p < 0.05$, **$p < 0.01$, ***$p < 0.001$, and ****$p < 0.0001$.
Additionally, refer to Figures S13–S18 and Table S2.

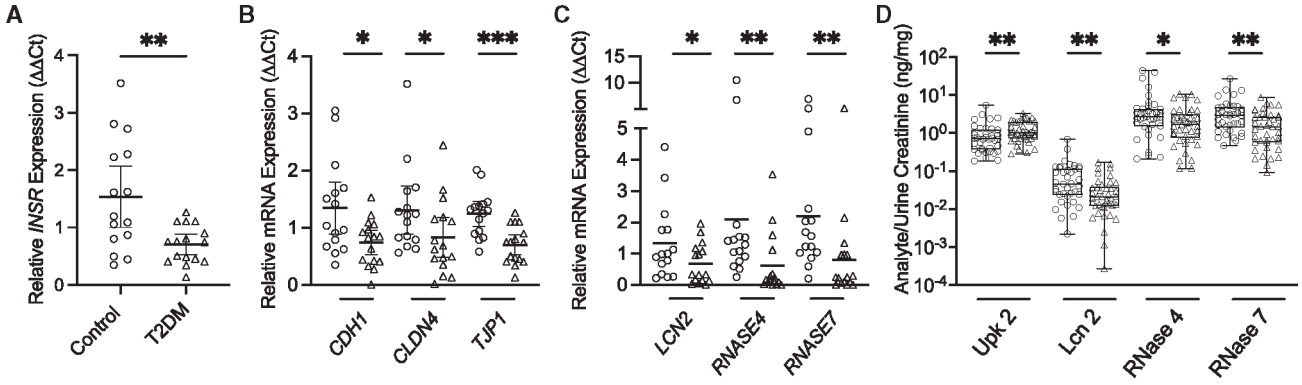

Figure 7. Youths with type 2 diabetes have suppressed urothelial and urinary antibacterial defenses

(A–C) Relative *INSR* (A), barrier gene (B), and antimicrobial peptide (C) mRNA expression in exfoliated urinary cells collected from healthy children and adolescents (open circles, n = 15) and youths with type 2 diabetes (open triangles, n = 16). Graphs show the mean and 95% confidence intervals.

(D) Urinary Upk2), Lcn 2, RNase 4, and RNase 7 concentrations, standardized to urine creatinine, in healthy controls (open circles, n = 38) and youth with type 2 diabetes (open triangles, n = 41). Center lines show the median values, box limits indicate the 25th and 75th percentiles, and whiskers show the minimum to maximum range.

Each symbol denotes a measurement in a different person. Asterisks denote significant p values for the indicated comparisons (Mann-Whitney U test). *p < 0.05, **p < 0.01, and ***p < 0.001. Additionally, refer to Table S3.

KEY RESOURCES TABLE

REAGENT or RESOURCE	SOURCE	IDENTIFIER
Antibodies		
Goat polyclonal anti-Uroplakin 3	Santa Cruz Biotechnology	Cat#sc-9882; RRID: AB_2289903
Rabbit polyclonal anti-PTP1B	Sigma-Aldrich	Cat#SAB4502525; RRID: AB_10761055
Rabbit polyclonal anti-Keratin 5	BioLegend	Cat#905501; RRID: AB_2565050
Rabbit polyclonal anti-IRα	Abcam	Cat#ab5500; RRID: AB_2296149
Rabbit polyclonal anti-NF-kB p65	Abcam	Cat#ab16502; RRID: AB_443394
Rabbit monoclonal anti-P-NF-kB p65 (ser536)	Cell Signaling	Cat#3033; RRID: AB_331284
Rabbit monoclonal anti-P-IGF1Rβ (tyr1135/1136)/IRβ (tyr1150/1151)	Cell Signaling	Cat#3024; RRID: AB_331253
Rabbit monoclonal anti-P-AKT (ser473)	Cell Signaling	Cat#4060; RRID: AB_2315049
Mouse monoclonal anti-IkBa	Cell Signaling	Cat#4814; RRID: AB_390781
Rabbit monoclonal anti-E-cadherin	Cell Signaling	Cat#3195; RRID: AB_2291471
Rabbit polyclonal anti-ZO-1	Invitrogen	Cat#61-7300; RRID: AB_2533938
Mouse monoclonal anti-Claudin 4	Invitrogen	Cat#32-9400; RRID: AB_2533096
Rabbit polyclonal anti-Claudin 8	Invitrogen	Cat#40-0700Z; RRID: AB_2533445
Rabbit monoclonal anti-GAPDH	Cell Signaling	Cat#5174; RRID: AB_10622025
Rabbit polyclonal anti-RFP/tdTomato	Rockland Immunochemicals Inc.	Cat#600-401-379; RRID: AB_2209751
Alexa Fluor® 488 AffiniPure Donkey Anti-Goat IgG	Jackson ImmunoResearch Laboratories	Cat#705-545-003; RRID: AB_2340428
Cy™3 AffiniPure F(ab')$_2$ Fragment Donkey Anti-Rabbit IgG	Jackson ImmunoResearch Laboratories	Cat#711-166-152; RRID: AB_2313568
Goat Anti-rabbit IgG, HRP linked secondary antibody	Cell Signaling	Cat#7074; RRID: AB_2099233
Rabbit IgG	Cell Signaling	Cat#2729; RRID: AB_1031062
Rabbit Histone H3	Cell Signaling	Cat#4620; RRID: AB_1904005
Alexa Fluor® 700 anti-mouse/human CD11b	BioLegend	Cat#101222; RRID: AB_493705
Brilliant Violet 785™ anti-mouse CD45 Antibody	BioLegend	Cat#103149; RRID: AB_2564590
PE anti-mouse CX3CR1	BioLegend	Cat#149006; RRID: AB_2564315
Brilliant Violet 650™ anti-mouse Ly-6G	BioLegend	Cat#127641; RRID: AB_2565881
eFluor™ 450, monoclonal antibody (HK1.4), Ly-6C	Invitrogen	Cat#48-5932-82; RRID: AB_10805519
Purified anti-mouse CD16/32	BioLegend	Cat#101301; RRID: AB_312800
APC Monoclonal antibody (M5/114.15.2) MHC Class II (I-A/I-E)	eBioscience	Cat#17-5321-81; RRID: AB_1548783
Bacterial and virus strains		
Uropathogenic *Escherichia coli* UTI89	Provided by Dr. Scott J. Hultgren	Hultgren et al.[69]
Biological samples		
Human urine from children and adolescents	This paper	This paper
Chemicals, peptides, and recombinant proteins		

REAGENT or RESOURCE	SOURCE	IDENTIFIER
Absolute Blue QPCR SYBR Mix	Thermo-Fisher	Cat#AB4322B
Alfa Aesar™ D-(–)-Tartaric Acid, 99%	Fisher Scientific	Cat#AAA1126414
Assay Assure	Thermo-Fisher	Cat#14103
DharmaFECT transfection reagent	Dharmacon	Cat#T-2001-02
OSI-906	Selleckchem	Cat#S1091
Gill's Hematoxylin I	Thermo Fisher Scientific	Cat#245-653
Human Insulin	Sigma-Aldrich	Cat#I9278
Lipofectamine	Thermo-Fisher	Cat#15338100
Low molecular weight FITC-conjugated dextran	Sigma-Aldrich	CAS#60842-46-8
OSI-906	Selleckchem	Cat#S1091
Low molecular weight FITC-conjugated dextran	Sigma-Aldrich	CAS#60842-46-8
LIVE/DEAD™ Fixable Blue Dead Cell Stain Kit, for UV excitation	Thermo-Fisher	Cat#L23105
Tamoxifen	Cayman Chemical	Cat#13258
Collagenase Type I	Sigma-Aldrich	Cat#SCR103
DMEM/F-12	Gibco	Cat#11320033
HEPES	Gibco	Cat#15630080
Critical commercial assays		
Ultra-sensitive mouse insulin ELISA	Crystal Chem	Cat#90080
Creatinine ELISA	Oxford Biomedical Research	SKU: CR01
Human lipocalin 2 ELISA	Abcam	Cat#Ab113326
Human RNase 4 ELISA	Mybiosource	Cat#MBS3804089
Human RNase 7 ELISA	Hycult Biotech	Cat#HK371-02
Human Uroplakin 2 ELISA	Lifespan Biosciences	Cat#LS-F25495
RNAscope™ 2.5 HD Duplex Assay	Advanced Cell Diagnostics	Cat#322436
RNA-Protein Co-detection Ancillary Kit	Advanced Cell Diagnostics	Cat#323180
Insr-C2 prob	Advanced Cell Diagnostics	Cat#1041961-C2
Polr2A-C2 prob	Advanced Cell Diagnostics	Cat#321651-C2
DapB-C2 prob	Advanced Cell Diagnostics	Cat#320751-C2
Dual-Glo Luciferase Assay Kit	Promega	Cat#E2920
SimpleChIP Enzymatic Chromatin IP Kit	Cell Signaling	Cat#9003
RNeasy Micro Kit	Qiagen	Cat#74004
RNeasy Plus Mini Kit	Qiagen	Cat#74134
Verso cDNA synthesis kit	Thermo-Fisher	Cat#AB1453A
RT2 First Strand Kit	Qiagen	Cat#330404
Mouse Antibacterial Response Arrays	Qiagen	Cat#PAMM-148Z
Experimental models: Cell lines		
Human 5637	ATCC	Cat#HTB-9; RRID:CVCL_0126
Human T24	ATCC	Cat#HTB-4; RRID:CVCL_0554

REAGENT or RESOURCE	SOURCE	IDENTIFIER
Primary human urothelial cells (HBLAK)	CELLnTEC Advanced Cell Systems	Cat#HBLAK; RRID:CVCL_JQ59
Experimental models: Organisms/strains		
Mouse: *ob/ob*: B6.Cg-*Lep*^{ob}/J	The Jackson Laboratory	JAX:006494
Mouse: PTP1B: B6.129S4-*Ptpn1*^{tm1Bbk}/Mmjax	The Jackson Laboratory	JAX: 012677
Mouse: Ins fl/fl: B6.129S4 (FVB)-*Insr*^{tm1Khn}/J	The Jackson Laboratory	JAX:006955
Mouse: Tdt: B6.Cg-Gt(ROSA) *26Sor*$^{tm14CAG-tdTomato)Hze}$/J	The Jackson Laboratory	JAX: 007914
Mouse: UPK2 iCre: B6; CBA-Tg(Upk2-icre/ERT2)1Ccc/J	The Jackson Laboratory	JAX:024768
Mouse: Krt5 iCre: B6N.129S6(Cg)-*Krt5*$^{tm1.1(cre/ERT2)Blh}$/J	The Jackson Laboratory	JAX:029155
Mouse: C3H/HeOuJ	The Jackson Laboratory	JAX: 000635
Oligonucleotides		
SMARTpool: ON-TARGETplus *INSR* siRNA	Horizon Discovery Ltd, Dharmacon.	Cat#L-003014-00-0005
SMARTpool: ON-TARGETplus *PTP1B* siRNA	Horizon Discovery Ltd, Dharmacon	Cat#L-003529-00-0005
SMARTpool: ON-TARGETplus *AKT1* siRNA	Horizon Discovery Ltd, Dharmacon	Cat# L-003000-00-0005
SMARTpool: ON-TARGETplus *NFKB1* siRNA	Horizon Discovery Ltd, Dharmacon	Cat#L-003520-00-0005
SMARTpool: ON-TARGETplus *CDH1* siRNA	Horizon Discovery Ltd, Dharmacon	Cat#L-003877-00-0005
SMARTpool: ON-TARGETplus *CLDN4* siRNA	Horizon Discovery Ltd, Dharmacon	Cat#L-013612-00-0005
SMARTpool: ON-TARGETplus *TJP1* siRNA	Horizon Discovery Ltd, Dharmacon	Cat#L-007746-00-0005
Primers for mouse data, see Table S3	This paper	This paper
Primers for human data and ChIP, see Table S4	This paper	This paper
Recombinant DNA		
Firefly luciferase NF-κB reporter plasmid pGL4.32[luc2P/NFκB-RE/Hygro]	Promega	Cat#E8491
pRL-CMV Renilla luciferase plasmid	Promega	Cat#E2261
Software and algorithms		
GeneGlobe Data Analysis Center	Qiagen	https://geneglobe.qiagen.com/us/analyze
FlowJo Software	BD Biosciences	https://www.flowjo.com/
Other		
Nikon Ti2-E microscope and DS-RI2 camera	Nikon Instruments Inc.	https://www.microscope.healthcare.nikon.com/en_EU/
aa Hitachi H-7650 microscope	Hitachi High-Technologies Corp.	https://www.hitachi-hightech.com/us/en/
BD™ LSR II Flow Cytometer	BD Biosciences	https://www.bdbiosciences.com/en-us

REAGENT or RESOURCE	SOURCE	IDENTIFIER
Spectramax M2 microplate reader	Molecular Devices	https://www.moleculardevices.com/
Veritas Microplate Luminometer	Turner BioSystems	https://www.turnerbiosystems.com/
7500 Real-Time PCR System	Applied Biosystems	https://www.thermofisher.com/us/en/home/brands/applied-biosystems.html
CountBright™ Absolute Counting Beads, for flow cytometry	Thermo-Fisher	Cat#C36950
AlphaTrak2 glucose monitoring system	Abbott Point of Care	https://www.abbott.com/
Chemstrip 2 GP	Roche Diagnostics	Cat#11895397